Molecular Cell

Short article

Delayed protein translocation protects mitochondria against toxic CAT-tailed proteins

Graphical abstract

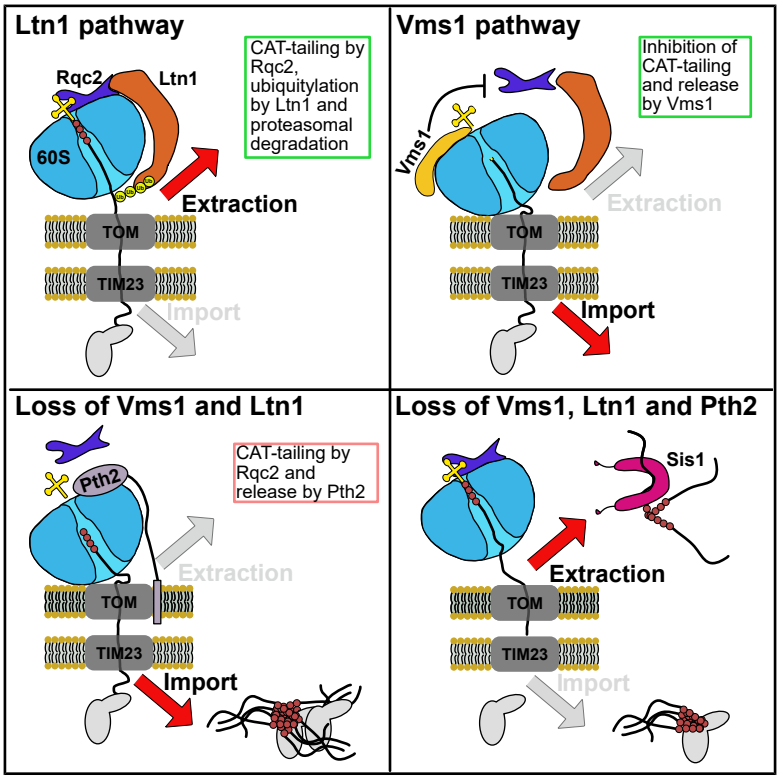

Highlights

- MitoRQC prevents the accumulation of toxic, mitochondria-localized CAT-tailed proteins
- A genome-wide screen identifies Pth2 as a peptidyl-tRNA hydrolase within mitoRQC
- Pth2 affects the import of CAT-tailed proteins and their access to the cytosolic QC network
- Delayed import, in general, protects mitochondria against toxic CAT-tailed proteins

Authors

Nils Bertram, Toshiaki Izawa, Felix Thoma, ..., Christof Osman, Walter Neupert, Dejana Mokranjac

Correspondence

mokranjac@bio.lmu.de

In brief

mitoRQC protects mitochondria against toxic CAT-tailed proteins. Using a genome-wide screen, Bertram et al. identify Pth2 as a peptidyl-tRNA hydrolase within mitoRQC. Pth2 modulates the import of CAT-tailed proteins and their access to the cytosolic QC network. Other hits from the screen show that, generally, delayed import protects mitochondria against toxic CAT-tailed proteins.

Bertram et al., 2025, Molecular Cell *85*, 4082–4092
November 6, 2025
https://doi.org/10.1016/j.molcel.2025.09.030

CellPress

CellPress
OPEN ACCESS

Molecular Cell

Short article

Delayed protein translocation protects mitochondria against toxic CAT-tailed proteins

Nils Bertram,[1] Toshiaki Izawa,[2,7] Felix Thoma,[1,3] Serena Schwenkert,[4] Stéphane Duvezin-Caubet,[5] Sae-Hun Park,[6] Nikola Wagener,[2] Anne Devin,[5] Christof Osman,[1] Walter Neupert,[2] and Dejana Mokranjac[1,8,*]

[1]LMU Munich, Faculty of Biology, Cell Biology, 82152 Martinsried, Germany
[2]LMU Munich, Faculty of Medicine, BMC-Cell Biology, 82152 Martinsried, Germany
[3]Graduate School Life Science Munich, 82152 Martinsried, Germany
[4]LMU Munich, Faculty of Biology, MSBioLMU, 82152 Martinsried, Germany
[5]Université Bordeaux, CNRS, IBGC, UMR 5095, 33000 Bordeaux, France
[6]Max Planck Institute of Biochemistry, Department of Cellular Biochemistry, 82152 Martinsried, Germany
[7]Present address: Graduate School of Life Science, University of Hyogo, Ako-gun, Hyogo 678-1297, Japan
[8]Lead contact
*Correspondence: mokranjac@bio.lmu.de
https://doi.org/10.1016/j.molcel.2025.09.030

SUMMARY

Ribosome-associated protein quality control (RQC) protects cells against the toxic effects of faulty polypeptides produced by stalled ribosomes. However, mitochondria are vulnerable to C-terminal alanyl and threonyl (CAT)-tailed proteins that are generated in this process, and faulty nuclear-encoded mitochondrial proteins are handled by the recently discovered mitoRQC. Here, we performed a genome-wide screen in yeast to identify additional proteins involved in mitoRQC. We found that peptidyl-tRNA hydrolase 2 (Pth2), present in the mitochondrial outer membrane, influences aggregation of CAT-tailed proteins without majorly affecting the CAT-tailing process itself. Peptidyl-tRNA hydrolase activity is essential during this process, yet the activity of Pth2 can be substituted by another peptidyl-tRNA hydrolase upon proper localization. Our data suggest that Pth2 acts by modulating protein translocation and that the mitochondrial proteostasis network is relieved through increased access of CAT-tailed proteins to cytosolic chaperones. Other hits obtained in the screen show that, in general, delayed protein translocation protects mitochondria against toxic CAT-tailed proteins.

INTRODUCTION

Defective proteins are constantly generated at a low rate during translation due to, e.g., mutations or damage to the mRNA or the ribosome. These aberrant nascent chains can aggregate, sequestering chaperones and inducing proteotoxic stress.[1,2] To prevent protein toxicity at an early stage, the ribosome-associated protein quality control (RQC) system monitors and degrades translation products that emerge from stalled ribosomes.[3–7] After dissociation of the stalled 80S ribosome,[8–10] the 60S subunit, with associated peptidyl-tRNA, is recognized by Rqc2, which then recruits E3 ubiquitin ligase Ltn1.[11–14] Ltn1 ubiquitylates nascent chains at lysine residues present in close proximity to the ribosomal exit tunnel.[12,13,15] Aided by Rqc1, together with Cdc48 and its cofactors, ubiquitylation leads to extraction of nascent chains and their subsequent degradation by the proteasome.[11,16,17] Rqc2 also has the ability to noncanonically elongate nascent chains by adding C-terminal alanine and threonine residues in a template- and 40S-independent manner.[14,18–21] This modification, termed C-terminal alanyl and threonyl (CAT) tailing, facilitates further ubiquitylation by Ltn1 by extruding additional lysine residues from the ribosomal exit tunnel.[22] CAT tails were shown to dislodge nascent chains from the ribosome catalytic centre[23] and serve as degrons in different organisms[24–27]; however, they also render proteins aggregation prone, leading to formation of SDS-insoluble aggregates.[20,28–30]

RQC acting on stalled ribosomes engaged in synthesis of nuclear-encoded mitochondrial proteins is complicated by the presence of N-terminal mitochondrial targeting sequences (MTSs).[29] The MTSs can already engage with mitochondrial protein translocases, the translocase of the outer mitochondrial membrane (TOM) complex in the outer and the translocase of the inner mitochondrial membrane 23 (TIM23) complex in the inner membrane, and initiate translocation before the nascent chain is released from the 60S subunit. This results in apposition of 60S with the TOM complex, reducing Ltn1's access to the nascent chains and hindering their ubiquitylation and subsequent extraction and degradation in the cytosol.[29] However, CAT tailing can still occur, eventually resulting in the import of

CellPress
OPEN ACCESS

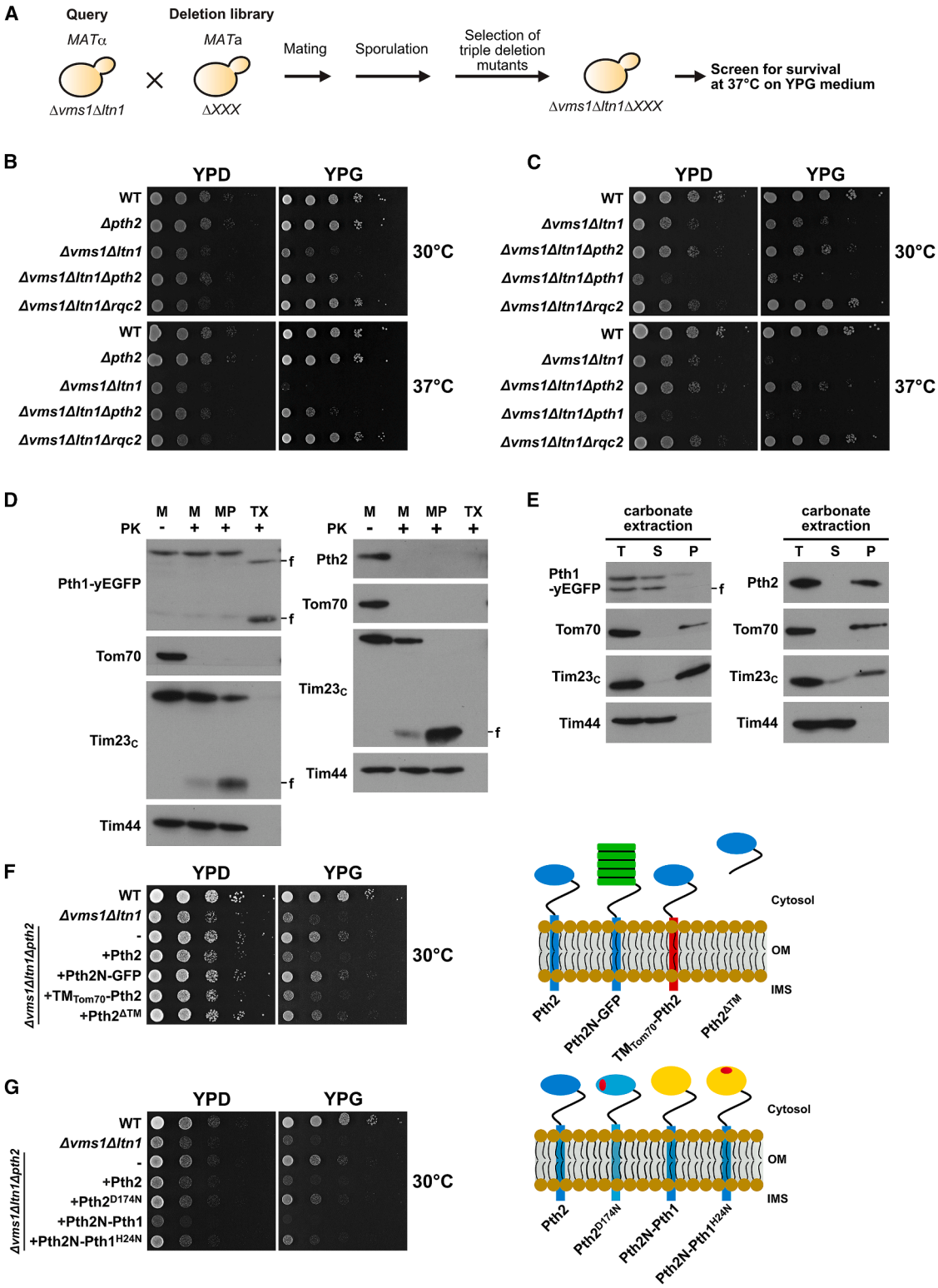

Figure 1. Pth2 is a peptidyl-tRNA hydrolase involved in yeast mitoRQC

(A) Schematic of the synthetic genetic array analysis.

(B) Ten-fold serial dilutions of the indicated cells were spotted on plates containing fermentable (YPD) or non-fermentable carbon sources (YPG) and incubated at indicated temperatures.

(legend continued on next page)

CAT-tailed proteins into mitochondria.[25,29] Mitochondria were recently shown to be especially sensitive to CAT-tailed proteins, leading to a collapse of the mitochondrial proteostasis network, compromising mitochondrial function, and ultimately resulting in cell death.[29] Therefore, mitochondria rely on the protective function of the cytosolic endonuclease Vms1,[31] which acts as a safeguard by halting CAT tailing, through both peptidyl-tRNA cleavage[32,33] and displacement of Rqc2 from the 60S subunit,[29,34] leading to the release of aberrant—but non-CAT-tailed—proteins into mitochondria. This RQC pathway acting on the mitochondrial surface is termed mitochondrial RQC (mitoRQC).[29]

To identify additional proteins involved in mitoRQC, we conducted genome-wide screens in yeast. We identified peptidyl-tRNA hydrolase 2 (Pth2), a functionally poorly characterized peptidyl-tRNA hydrolase in the mitochondrial outer membrane,[35–37] as a release factor of CAT-tailed proteins arrested in the TOM complex. Data presented here indicate that Pth2 does not influence CAT tailing of nascent chains but rather their translocation into mitochondria, providing more time for the cytosolic proteostasis network to deal with the mitoRQC substrates. Deletions of nonessential TOM and TIM23 components had similar effects, suggesting that delaying protein translocation is a general mechanism protecting mitochondria against toxic CAT-tailed proteins.

RESULTS AND DISCUSSION

Pth2 is involved in mitoRQC

To identify novel proteins involved in mitoRQC, we employed genome-wide screens in the yeast *Saccharomyces cerevisiae*, looking for components able to restore growth of *Δvms1Δltn1* cells[29] on non-fermentable medium at 37°C. A high-copy suppressor screen did not identify any obvious novel candidates, though Ltn1 and Vms1 were both repeatedly identified (data not shown). In the second approach, we mated *Δvms1Δltn1* cells with the yeast deletion library and screened for triple mutants that are viable under the screening conditions (Figure 1A). Rqc2 was present among the identified candidates, confirming the validity of the approach (Table S1). One candidate, Pth2, drew our attention as it was previously shown to be an outer mitochondrial membrane protein interacting with the TOM complex,[37] and its human homolog, PTRH2, was implicated in a number of human disorders.[38] To validate the results obtained in the screen, we deleted *PTH2* in wild-type (WT), *Δvms1*, *Δltn1*, and *Δvms1Δltn1* strains and conducted comprehensive growth analyses on fermentable (YPD) and non-fermentable (YPG) media. As in the screen, additional deletion of *PTH2* restored growth of *Δvms1Δltn1* cells on both media, though not to the same extent as deletion of *RQC2* did (Figure 1B). We observed no growth defects in any of the single-deletion strains nor in the *Δltn1Δpth2* and *Δvms1Δpth2* double mutants under tested conditions (Figures 1B, S1A, and S1B).

Mitochondria contain an additional Pth, Pth1,[36] whose mammalian homolog, PTRH1, was recently implicated in the RQC pathway in mammalian cells.[33] In addition, bacterial Pth was recently shown to release stalled nascent chains in a C-terminal-tail-dependent manner.[23] Interestingly, we did not identify Pth1 in the screen. To exclude potential artefacts of high-throughput screening, we deleted *PTH1* in both WT and *Δvms1Δltn1* cells. In contrast to *PTH2* deletion, deletion of *PTH1* did not improve growth of *Δvms1Δltn1* cells but rather aggravated the already severe growth defect (Figures 1C and S1C). This observation can be explained by the different subcellular localizations of the two enzymes, supporting their involvement in different pathways. Whereas Pth2 is integrated in the outer membrane and exposes its catalytic domain to the cytosol, Pth1 is a soluble protein in the matrix (Figures 1D and 1E). Thus, Pth2, and not Pth1, is involved in mitoRQC in yeast. Whether PTRH1 localizes to the mitochondrial surface, under normal or stress conditions, remains to be determined.

Based on the primary sequence conservation, Pth2 was previously divided into N- and C-terminal regions[35,39] (Figure S1D). Though the N-terminal region lacks conservation on the primary sequence, it contains a predicted transmembrane domain in all examined orthologs (Figures S1D and S1E). The C-terminal region is highly conserved among different eukaryotic species (Figure S1D). To investigate involvement of the two regions within mitoRQC, we generated different constructs (Figures 1F, 1G, and S1F). The WT Pth2 construct, expressed under the control of the *PTH2* promoter and genomically integrated in *Δvms1Δltn1Δpth2* cells, reconstituted the *Δvms1Δltn1* phenotype (Figures 1F, 1G, S1G, S1I, and S1K), validating the approach taken. The substitution of the entire C-terminal region of Pth2 with superfolded GFP (Pth2N-GFP) led to a strain that phenocopied *Δvms1Δltn1Δpth2*, suggesting that this construct is a functionally inactive form of Pth2 (Figures 1F, S1F, S1G, and S1I). In contrast, the replacement of the transmembrane domain of Pth2 with that of the mitochondrial outer membrane protein Tom70 (TM_{Tom70}-Pth2), to maintain the localization of the C-terminal region of the protein, replicated the effect of expressing WT Pth2, suggesting that the C-terminal region of Pth2 plays an essential role in mitoRQC (Figures 1F, S1F, S1G, and S1I). The construct lacking the transmembrane domain ($Pth2^{\Delta TM}$), which was previously shown to reside in the cytosol,[37] showed an intermediate phenotype (Figures 1F, S1F, S1G, and S1I).

To assess whether Pth2 catalytic activity is important within mitoRQC, we introduced a point mutation ($Pth2^{D174N}$) in its catalytic site that was previously demonstrated to impair the Pth activity of Pth2.[39] *Δvms1Δltn1Δpth2* cells expressing $Pth2^{D174N}$ grew better

(C) Growth of indicated yeast strains was analyzed as in (B).
(D) Isolated mitochondria (M), mitoplasts (MP) prepared by osmotic shock, and Triton-solubilized mitochondria (TX) were treated with Proteinase K (PK), where indicated. Samples were analyzed by SDS-PAGE and western blot. Tom70, Tim23, and Tim44 were used as markers for outer membrane, inner membrane, and matrix, respectively. f-stable fragments of Tim23 in the inner membrane and of Pth1-yEGFP. Pth1-yEGFP was detected using GFP antibody.
(E) Total (T), supernatant (S), and pellet (P) fractions of carbonate extraction were analyzed by SDS-PAGE and western blotting.
(F and G) Growth of indicated yeast strains was analyzed as in (B) (left). Cartoons of Pth2 constructs (right).
See also Figure S1 and Table S1.

CellPress
OPEN ACCESS

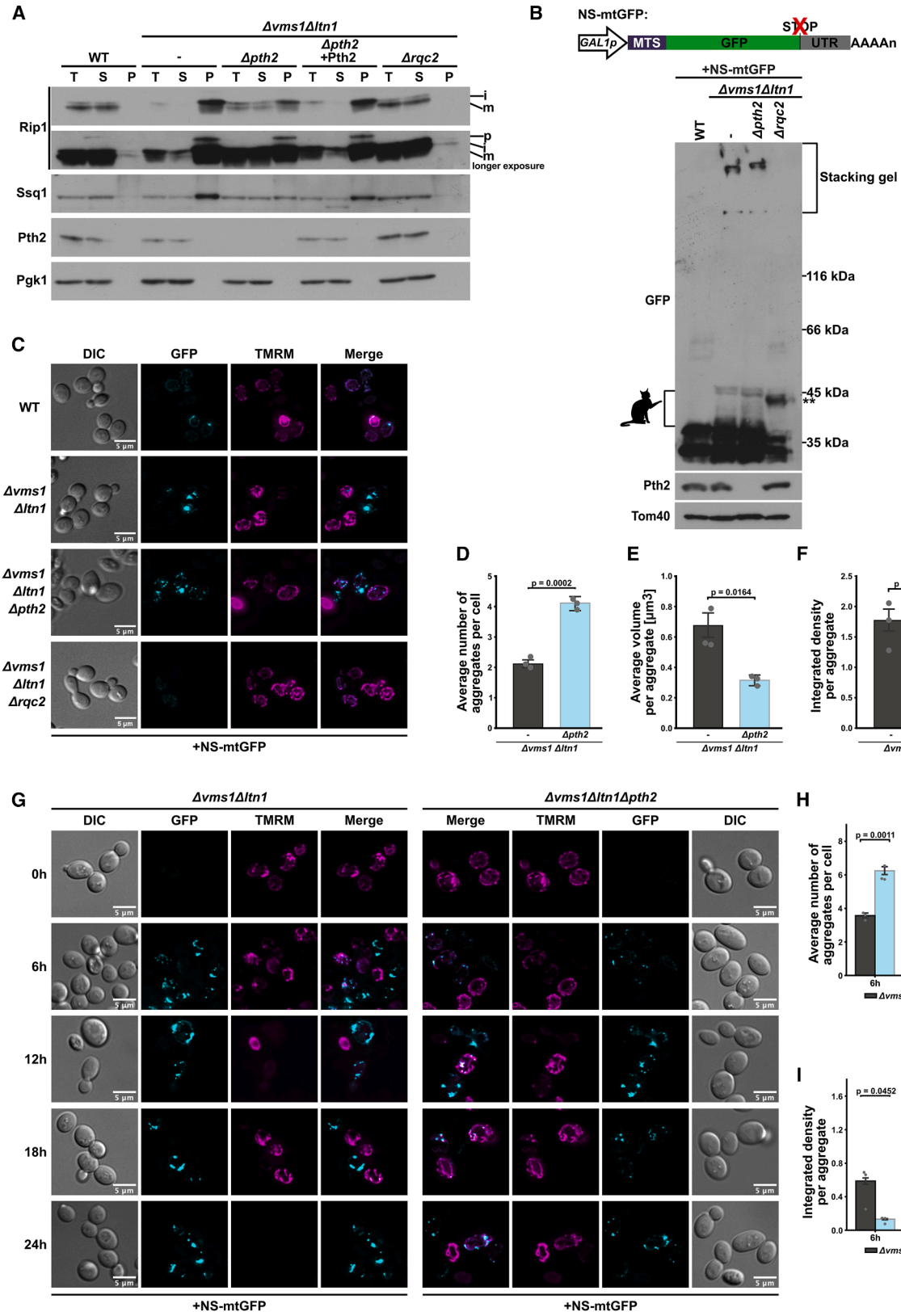

(legend on next page)

than *Δvms1Δltn1* cells (Figures 1G, S1D, S1F, S1H, and S1K), strongly suggesting that the Pth activity of Pth2 is toxic in *Δvms1Δltn1* cells. To investigate whether this function is exclusive to Pth2 or whether another Pth could substitute for it, we fused Pth1 to the N-terminal region of Pth2 to ensure the localization of Pth1 in the outer membrane (Figures 1G and S1F). *Δvms1Δltn1Δpth2* cells expressing Pth2N-Pth1 grew even worse than *Δvms1Δltn1* cells (Figures 1G and S1K). However, a point mutant that abrogates the catalytic activity of Pth1 (Pth2N-Pth1^{H24N})[33] improved cell growth (Figures 1G, S1F, S1J, and S1K).

Taken together, these data indicate that Pth2 is involved in mitoRQC pathway as a peptidyl-tRNA hydrolase. The function of Pth2 can, however, be substituted by another peptidyl-tRNA hydrolase, upon proper localization. This finding is in agreement with a previously demonstrated remarkable functional conservation of peptidyl-tRNA hydrolases—both Pth1 and Pth2 can substitute for the essential enzyme in bacteria.[36,39]

Absence of Pth2 reduces aggregate formation but does not affect CAT tailing

Toxicity associated with mitoRQC dysfunction in *Δvms1Δltn1* cells is primarily attributed to CAT-tail-dependent aggregation of proteins within the mitochondrial matrix.[29] Indeed, expression of mitochondrially targeted GFP variants extended with 10 or 15 AT repeats, to mimic CAT tails without initiating an RQC response, led to the formation of protein aggregates and inhibited growth of WT cells, especially with the longer CAT tail (Figures S2A–S2D). To investigate whether the absence of Pth2 mitigates protein aggregation, we isolated detergent-insoluble protein aggregates from the cell lysates of WT, *Δvms1Δltn1*, *Δvms1Δltn1Δpth2*, *Δvms1Δltn1Δrqc2*, and *Δvms1Δltn1Δpth2* cells with reintroduced Pth2. Rieske Fe-S protein Rip1, which was previously used as a marker for aggregation of mitochondrial proteins,[29] was present in the soluble fraction and was almost completely processed to its mature form in WT cells but was exclusively found in the aggregate fraction and was processed only to its intermediate form in *Δvms1Δltn1* cells (Figure 2A), as described previously.[29] Whereas additional deletion of *RQC2* in *Δvms1Δltn1Δrqc2* cells fully restored both the solubility and processing of Rip1, in *Δvms1Δltn1Δpth2* cells only part of Rip1 was fully processed and soluble (Figure 2A). A fraction of the intermediate form of Rip1 was, however, also present in the soluble form. The precursor form of Rip1 did not increase in *Δvms1Δltn1Δpth2* cells. In *Δvms1Δltn1Δpth2* cells with reintroduced Pth2, Rip1 behaved essentially the same as in *Δvms1Δltn1*. Ssq1, an Hsp70 chaperone in the mitochondrial matrix, behaved similarly to Rip1. In contrast, cytosolic protein Pgk1 was always present in the soluble fraction. In agreement with these findings, assembly of ATP synthase and activity of the respiratory chain, which are essentially absent in *Δvms1Δltn1*, were partially restored in *Δvms1Δltn1Δpth2* cells (Figures S2E–S2H). Thus, additional deletion of *PTH2* partially improved solubility of mitochondrial proteins and restored mitochondrial physiology of *Δvms1Δltn1* cells, correlating well with the observed partial growth rescue.

To test whether Pth2 affects CAT tailing, we expressed a mitochondrially targeted version of GFP lacking the stop codon (non-stop mitochondrially targeted GFP, NS-mtGFP) from an inducible promoter (Figure 2B). Translation of mRNAs lacking the stop codon results in proteins with a C-terminal poly-lysine stretch due to a partial translation of polyA tails. These poly-lysine stretches stall the NS proteins in the ribosomal exit tunnel, making them substrates of RQC.[40] CAT tailing of this construct, visible as a smear running slower than the monomeric GFP,[16,28,29] was obvious in cell extracts of *Δvms1Δltn1* and *Δvms1Δltn1Δpth2*. Furthermore, high-molecular-weight, SDS-insoluble aggregates were detected in the same samples in the stacking gel (Figure 2B). Neither CAT tailing nor aggregation of GFP was detected in WT or *Δvms1Δltn1Δrqc2* cells. Therefore, Pth2 does not appear to majorly influence CAT tailing.

To further investigate the protein aggregates present in *Δvms1Δltn1* and *Δvms1Δltn1Δpth2* cells, we used wide-field fluorescence microscopy. Twenty hours after the induction of NS-mtGFP expression, only a faint GFP signal, colocalizing with mitochondrial tubules, was detected in WT and *Δvms1Δltn1Δrqc2* cells (Figures 2C and S2I). In contrast, *Δvms1Δltn1* and *Δvms1Δltn1Δpth2* cells clearly contained GFP aggregates, which appeared smaller and less intense in the latter (Figure 2C). Quantification of number, size, and intensity of the aggregates (Figures 2D–2F) confirmed our assessments. Filter trap assay corroborated the presence of smaller amounts of SDS-insoluble aggregates in *Δvms1Δltn1Δpth2* than in *Δvms1Δltn1* cells (Figures S2J and S2K). The membrane-potential-sensitive dye TMRM[41] effectively stained mitochondria in the majority of WT and *Δvms1Δltn1Δrqc2* cells, but not in cells with large GFP aggregates, indicating a breakdown of membrane potential (not quantified), in agreement with the mitochondrial physiology measurements. To assess the kinetics of aggregate formation in *Δvms1Δltn1* and *Δvms1Δltn1Δpth2* cells, we analyzed cells before, and 6, 12, 18, and 24 h after, NS-mtGFP induction. Whereas cells

Figure 2. Absence of Pth2 reduces aggregate formation but does not affect CAT tailing

(A) Total cell extracts (T) of cells grown in YPGal medium at 37°C were prepared and either directly analyzed by SDS-PAGE and western blot or first fractionated by centrifugation into supernatant (S), containing soluble proteins, and pellet (P), containing aggregated proteins. T and S, 10% of P. p, precursor; i, intermediate; and m, mature forms of Rip1.

(B) Scheme of the NS-mtGFP construct used (upper panel). Total cell extracts were prepared 20 h after induction of NS-mtGFP expression at 30°C and analyzed by SDS-PAGE and western blot. Stacking gel contains aggregated NS-mtGFP. Cat represents CAT tailed and ** an unclarified form of NS-mtGFP.

(C) Fluorescence microscopy of NS-mtGFP-expressing cells. Yeast cells were grown as in (B). Mitochondria were stained with TMRM. The GFP signal was scaled equally, and the TMRM signal was auto-adjusted.

(D–F) Quantification of microscopy images of *Δvms1Δltn1* and *Δvms1Δltn1Δpth2* cells from (C). Statistical analysis was performed by comparing the means of three biological replicates using a two-sided t test. Results are represented as mean with 95% confidence interval.

(G) Time-course fluorescence microscopy of *Δvms1Δltn1* and *Δvms1Δltn1Δpth2* cells upon induction of NS-mtGFP expression. Channels were adjusted as in (C).

(H and I) Quantification of microscopy images from (G), performed as in (D)–(F).

See also Figure S2.

before induction had no visible GFP signal, aggregates were visible in both strains 6 h post induction. The aggregates were smaller and less intense in *Δvms1Δltn1Δpth2* than in *Δvms1Δltn1* cells (Figure 2G). Overall, *Δvms1Δltn1* cells showed a time-dependent decrease in number of aggregates per cell, with a simultaneous increase in their intensity (Figures 2H and 2I). The number of aggregates per cell consistently remained larger in *Δvms1Δltn1Δpth2* than in *Δvms1Δltn1* cells, and their intensity was comparably lower at all time points analyzed (Figures 2G–2I).

In summary, deletion of *PTH2* reduced aggregate formation in *Δvms1Δltn1* cells but did not majorly affect CAT tailing.

Absence of Pth2 delays the import of CAT-tailed nascent chains

Building upon our finding that Pth2 functions as a Pth within mitoRQC, and on previous *in vitro* data indicating that Pth2 can release nascent chains from intrinsically destabilized 80S ribosomes[42] and PTRH2 from both 80S and 60S,[33] we analyzed whether NS-mtGFP-tRNA intermediates accumulate in the absence of Pth2 *in vivo*. In cell lysates prepared in the presence of an RNase inhibitor, we observed an additional GFP species migrating at approximately 50 kDa, which was weak in *Δvms1Δltn1Δpth2* cells and stronger in *Δvms1Δltn1Δrqc2* cells (Figure 3A). The same species was also present in *Δvms1Δpth2* cells, but not in either of the single mutants (Figure S3A), suggesting partially overlapping functions of Vms1 and Pth2 and potentially explaining the poor growth of *Δvms1Δpth2* cells upon overexpression of mitoRQC substrates (Figure S3B). Treatment with RNaseA completely removed this species, confirming its identity as peptidyl-tRNA.[17] Considering the difference in signal intensities of peptidyl-tRNA species in *Δvms1Δltn1Δpth2* and *Δvms1Δltn1Δrqc2* cells, it appears that, in the absence of both Vms1 and Pth2, another endonuclease and/or peptidyl-tRNA hydrolase can release nascent chains from the 60S subunit. However, neither Pth2 nor this additional enzyme seems to have access to non-CAT-tailed peptidyl-tRNAs, which accumulate in *Δvms1Δltn1Δrqc2* cells. Accumulation of peptidyl-tRNAs in *Δvms1Δltn1Δpth2* cells is likely underestimated here as it is unclear to what extent this species accumulates in the aggregate fraction. Strong accumulation of peptidyl-tRNAs observed in *Δvms1Δltn1Δrqc2* cells may explain why deletion of *RQC2* did not restore growth of *Δvms1Δltn1* cells upon induction of NS-mtGFP expression (Figure S3C)—CAT tailing may be crucial for ribosome recycling in the presence of overwhelming amounts of RQC substrates.

We next compared the interactomes of NS-mtGFP in *Δvms1Δltn1Δpth2* and *Δvms1Δltn1* cells. For this, we analyzed NS-mtGFP immunoprecipitates from the two strains by mass spectrometry (Figure 3B; Table S2). 60S ribosomal proteins predominantly clustered on the *Δvms1Δltn1Δpth2* side of the volcano plot, with 10%–30% enrichments indicating more stable interaction of NS-mtGFP with 60S in *Δvms1Δltn1Δpth2* cells. This finding is consistent with a reduced release of stalled nascent chains from the 60S subunit in the absence of Pth2. Moreover, the interactome of NS-mtGFP in *Δvms1Δltn1Δpth2* cells contained reduced levels of the majority of mitochondrial proteins—predominantly matrix proteins, including the chaperones Hsp60 and mtHsp70 (Figures 3B and 3C)—consistent with their decreased aggregation in these cells (Figures 2A–2F). One notable exception was Tom40, which was enriched in the interactome in *Δvms1Δltn1Δpth2* cells (Figure 3B). Increased association of NS-mtGFP with Tom40 in *Δvms1Δltn1Δpth2* cells, compared with *Δvms1Δltn1* cells, was confirmed by western blot (Figure 3C). Among the proteins with the highest enrichment in the NS-mtGFP interactome in *Δvms1Δltn1Δpth2* cells was Sis1 (Figure 3B), the cytosolic chaperone previously shown to interact with cytosolic CAT-tailed proteins.[18,28,43] We also validated this result using western blot (Figure 3C). Although Sis1 aggregation occurred in both *Δvms1Δltn1* and *Δvms1Δltn1Δpth2* cells, aggregated Sis1 was specifically bound to NS-mtGFP only in *Δvms1Δltn1Δpth2* cells (Figure 3C). These data indicate that the stalled nascent chains dwell longer in the TOM complex and have increased access to the cytosolic proteostasis network in *Δvms1Δltn1Δpth2* cells compared with *Δvms1Δltn1* cells.

Delayed translocation protects mitochondria against toxic CAT-tailed proteins

Our data suggest that the NS-mtGFP-tRNA intermediate bound to 60S is stabilized in the TOM pore in *Δvms1Δltn1Δpth2* cells, preventing its complete translocation. We therefore wondered whether delayed translocation of CAT-tailed proteins could be a general protective mechanism. To this end, we re-analyzed the list of candidates obtained in the screen, and, indeed, virtually all nonessential subunits of the TOM and TIM23 complexes were among the genes whose deletion restored the growth of *Δvms1Δltn1* cells (Table S1). We confirmed that additional deletions of *TOM6* from the TOM complex and *TIM21* from the TIM23 complex restored growth of *Δvms1Δltn1* cells essentially to WT levels on fermentable and non-fermentable media and at 30°C and 37°C (Figures 4A and 4B).

Based on the available data, we propose an updated model of mitoRQC (Figure 4C). Substrates of mitoRQC are faulty, nuclear-encoded mitochondrial proteins that are still bound to the 60S ribosomal subunit and accumulate in the TOM and TIM23 complexes on their way into mitochondria. In the absence of Vms1 and Ltn1, they are constantly CAT tailed by Rqc2. These CAT-tailed nascent chains are substrates of Pth2 in the outer membrane. Pth2, whose catalytic domain is connected to the outer membrane via a long and flexible linker (Figure S4), releases CAT-tailed nascent chains from the 60S subunit, allowing their import into mitochondria. However, once in the mitochondrial matrix, these CAT-tailed proteins aggregate, sequestering chaperones and resulting in mitochondrial toxicity. In the absence of Pth2, the release of CAT-tailed nascent chains is delayed and they remain longer in the TOM complex. Longer dwelling time in the TOM complex, likely accompanied by increased movement of the nascent chain within the translocation channel, provides more time and accessibility for the components of the cytosolic proteostasis network—including both the ubiquitin-proteasome system and chaperones such as Sis1—to act. The prolonged access of mitoRQC substrates to the cytosolic proteostasis network can also be achieved by lowering the activities of the TOM and TIM23 complexes. At the same time, delayed import of CAT-tailed proteins reduces their aggregation inside mitochondria, relieving the organellar proteostasis network and restoring mitochondrial function.

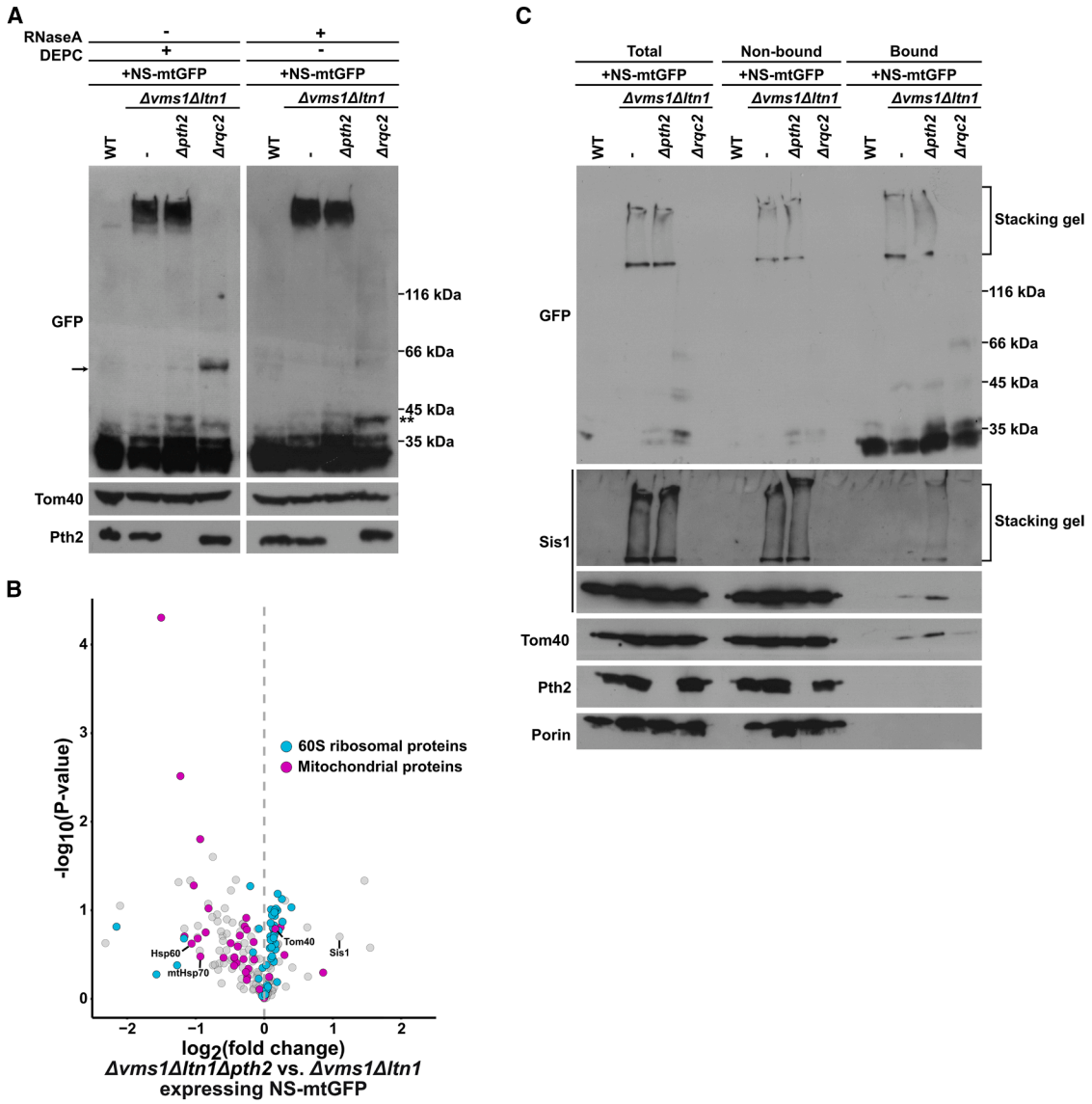

Figure 3. Absence of Pth2 delays import of CAT-tailed nascent chains

(A) Analysis of tRNA-linked NS-mtGFP. Cells were grown as in Figure 2B and lysed in either the presence of RNaseA or the RNase inhibitor DEPC. Lysates were analyzed by neutral pH SDS-PAGE and western blot. Arrow represents tRNA-NS-mtGFP conjugate and ** an unclarified form of NS-mtGFP.

(B) Volcano plot of NS-mtGFP interactors in *Δvms1Δltn1Δpth2* vs. *Δvms1Δltn1* cells. Yeast cells were grown as in Figure 2B. Lysates were immunoprecipitated with anti-GFP nanobodies followed by on-bead digestion and label-free quantification by mass spectrometry. 60S subunits are shown in blue and mitochondrial proteins in magenta.

(C) Cell lysates as in (B) were immunoprecipitated using anti-GFP nanobodies. Total (10%), non-bound (10%), and bound (100%) fractions were analyzed by SDS-PAGE and western blot with indicated antibodies.

See also Figure S3 and Table S2.

Limitations of the study

The physiological role of Pth2 and its substrate specificity, particularly in comparison to Vms1, remain to be further explored. The interplay of Pth2 with Ltn1 requires further investigation. Moreover, it remains unclear which components of the cytosolic proteostasis network are directly involved in the extraction of stalled nascent chains from the TOM complex in *Δvms1Δltn1Δpth2* cells. Subcellular localization of protein aggregates in *Δvms1Δltn1Δpth2* cells needs to be analyzed by higher-resolution techniques.

RESOURCE AVAILABILITY

Lead contact

Further information and requests for resources and reagents should be directed to, and will be fulfilled by, the lead contact, Dejana Mokranjac (mokranjac@bio.lmu.de).

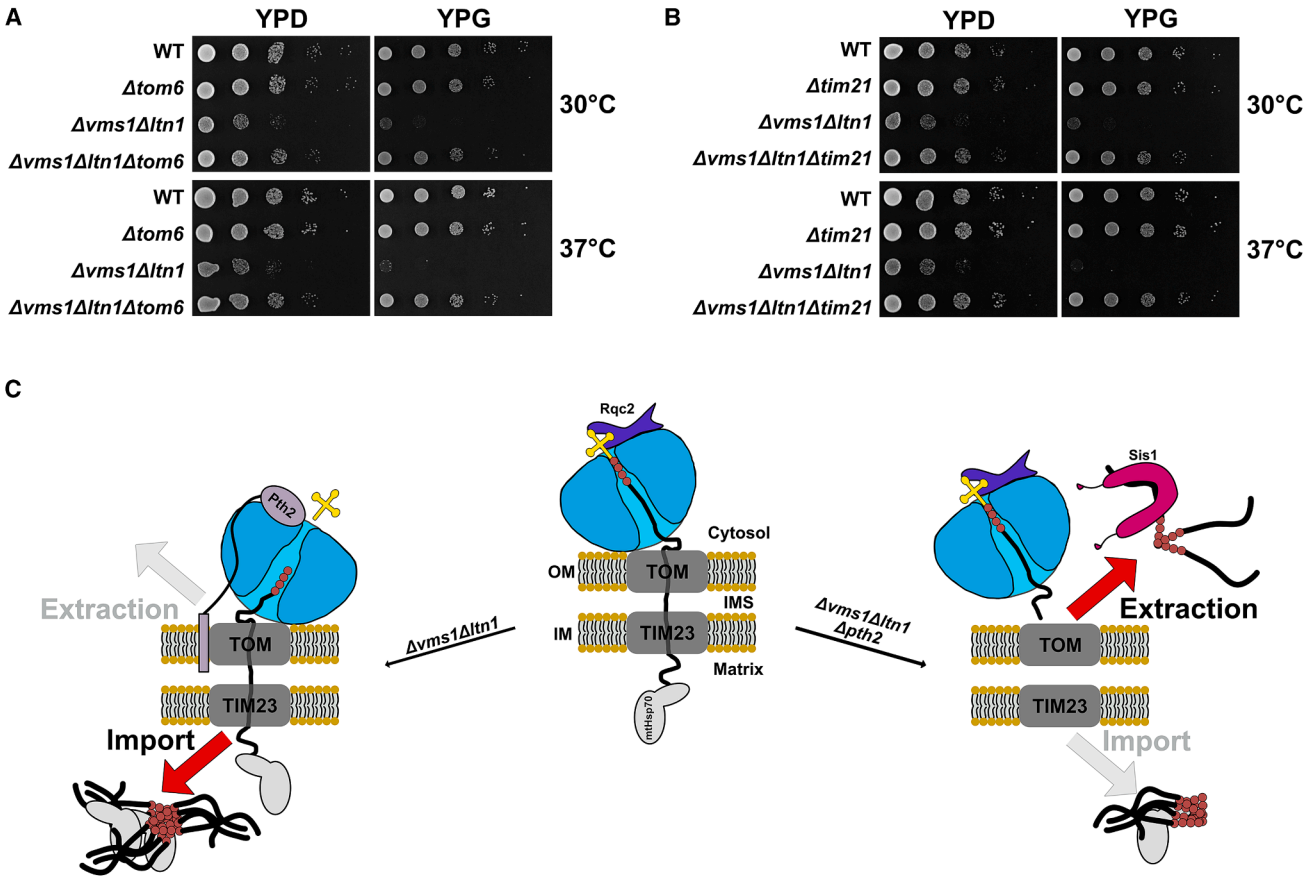

Figure 4. Delayed protein translocation protects mitochondria against toxic CAT-tailed proteins

(A and B) Growth of indicated yeast strains was analyzed as in Figure 1B.

(C) Updated model of mitoRQC. See text for details.

See also Figure S4.

Materials availability

Plasmids and yeast strains generated in this study will be available from the lead contact upon request.

Data and code availability

- The raw data of mass spectrometry were deposited in the PRIDE repository and are publicly available as of the date of publication under the accession number PRIDE: PXD057575.
- This paper does not report original code.
- Any additional information required to reanalyze the data reported in this paper is available from the lead contact upon request.

ACKNOWLEDGMENTS

We thank current and past members of the Mokranjac lab and Mitoclub for their support and stimulating discussions, Johannes Buchner for providing the antibody against Sis1, Roland Beckmann for critical comments, and F. Ulrich Hartl for his continuous support. We also thank Jochen Rech for his help with the original yeast screen and the Robotics Core Facility at the Max Planck Institute (MPI) of Biochemistry for support. This research was generously supported by the Deutsche Forschungsgemeinschaft (projects NE101/28-1 to W. N. and MO1944/2-1 and MO1944/3-1 to D.M.). N.B. is the recipient of a doctoral fellowship awarded by the Walter and Monika Neupert Foundation. F.T. and C.O. were supported by a Human Frontier Science Program research grant (RGP021/2023) and a Deutsche Forschungsgemeinschaft research grant (OS410/3-1). Collaboration between D.M. and S.D.-C. was supported by the LMU-Bordeaux Research Cooperation Program and Bay-France (FK-21-2023). S.D.-C. and A.D. are supported by CNRS. We acknowledge the contributions of Walter Neupert, who passed away during the course of this work.

AUTHOR CONTRIBUTIONS

Conceptualization, D.M., W.N., and N.B.; methodology, D.M., N.B., F.T., S.S., S.D.-C., S.-H.P., and A.D.; resources, D.M., W.N., C.O., S.-H.P., and A.D.; investigation, N.B., T.I., S.S., N.W., and S.D.-C.; formal analysis, N.B., T.I., F.T., S.S., and S.D.-C.; visualization, N.B., T.I., F.T., and S.D.-C.; supervision, D.M., W.N., S.-H.P., and C.O.; funding acquisition, D.M., W.N., C.O., S.D.-C., and A.D.; writing – original draft, D.M. and N.B. All authors discussed the results obtained and commented on the manuscript.

DECLARATION OF INTERESTS

The authors declare no competing interests.

STAR★METHODS

Detailed methods are provided in the online version of this paper and include the following:

- KEY RESOURCES TABLE
- EXPERIMENTAL MODEL AND STUDY PARTICIPANT DETAILS

- Yeast strains and plasmids
- METHOD DETAILS
  - Synthetic genetic array analysis
  - Analysis of growth of yeast cells
  - Submitochondrial localization
  - Total cell extracts
  - Protein aggregation assay
  - Filter trap assay
  - Blue Native-PAGE
  - Oxygen consumption assay
  - Determination of enzymatic activities
  - Peptidyl-tRNA accumulation assay
  - Immunoprecipitation of NS-mtGFP
  - LC-MS/MS analysis
  - Fluorescence microscopy
  - Pth2 antibody generation
- QUANTIFICATION AND STATISTICAL ANALYSIS

SUPPLEMENTAL INFORMATION

Supplemental information can be found online at https://doi.org/10.1016/j.molcel.2025.09.030.

Received: November 20, 2024
Revised: May 16, 2025
Accepted: September 26, 2025
Published: October 20, 2025

REFERENCES

1. Pilla, E., Schneider, K., and Bertolotti, A. (2017). Coping with Protein Quality Control Failure. Annu. Rev. Cell Dev. Biol. *33*, 439–465. https://doi.org/10.1146/annurev-cellbio-111315-125334.
2. Hipp, M.S., Kasturi, P., and Hartl, F.U. (2019). The proteostasis network and its decline in ageing. Nat. Rev. Mol. Cell Biol. *20*, 421–435. https://doi.org/10.1038/s41580-019-0101-y.
3. Filbeck, S., Cerullo, F., Pfeffer, S., and Joazeiro, C.A.P. (2022). Ribosome-associated quality-control mechanisms from bacteria to humans. Mol. Cell *82*, 1451–1466. https://doi.org/10.1016/j.molcel.2022.03.038.
4. Inada, T., and Beckmann, R. (2024). Mechanisms of Translation-coupled Quality Control. J. Mol. Biol. *436*, 168496. https://doi.org/10.1016/j.jmb.2024.168496.
5. Iyer, K.V., Müller, M., Tittel, L.S., and Winz, M.-L. (2023). Molecular Highway Patrol for Ribosome Collisions. Chembiochem *24*, e202300264. https://doi.org/10.1002/cbic.202300264.
6. Joazeiro, C.A.P. (2019). Mechanisms and functions of ribosome-associated protein quality control. Nat. Rev. Mol. Cell Biol. *20*, 368–383. https://doi.org/10.1038/s41580-019-0118-2.
7. Howard, C.J., and Frost, A. (2021). Ribosome-associated quality control and CAT tailing. Crit. Rev. Biochem. Mol. Biol. *56*, 603–620. https://doi.org/10.1080/10409238.2021.1938507.
8. Pisareva, V.P., Skabkin, M.A., Hellen, C.U.T., Pestova, T.V., and Pisarev, A.V. (2011). Dissociation by Pelota, Hbs1 and ABCE1 of mammalian vacant 80S ribosomes and stalled elongation complexes. EMBO J. *30*, 1804–1817. https://doi.org/10.1038/emboj.2011.93.
9. Shao, S., von der Malsburg, K., and Hegde, R.S. (2013). Listerin-Dependent Nascent Protein Ubiquitination Relies on Ribosome Subunit Dissociation. Mol. Cell *50*, 637–648. https://doi.org/10.1016/j.molcel.2013.04.015.
10. Shoemaker, C.J., Eyler, D.E., and Green, R. (2010). Dom34:Hbs1 promotes subunit dissociation and peptidyl-tRNA drop-off to initiate no-go decay. Science *330*, 369–372. https://doi.org/10.1126/science.1192430.
11. Defenouillère, Q., Yao, Y., Mouaikel, J., Namane, A., Galopier, A., Decourty, L., Doyen, A., Malabat, C., Saveanu, C., Jacquier, A., et al. (2013). Cdc48-associated complex bound to 60S particles is required for the clearance of aberrant translation products. Proc. Natl. Acad. Sci. USA *110*, 5046–5051. https://doi.org/10.1073/pnas.1221724110.
12. Lyumkis, D., Oliveira dos Passos, D., Tahara, E.B., Webb, K., Bennett, E.J., Vinterbo, S., Potter, C.S., Carragher, B., and Joazeiro, C.A.P. (2014). Structural basis for translational surveillance by the large ribosomal subunit-associated protein quality control complex. Proc. Natl. Acad. Sci. USA *111*, 15981–15986. https://doi.org/10.1073/pnas.1413882111.
13. Shao, S., Brown, A., Santhanam, B., and Hegde, R.S. (2015). Structure and assembly pathway of the ribosome quality control complex. Mol. Cell *57*, 433–444. https://doi.org/10.1016/j.molcel.2014.12.015.
14. Shen, P.S., Park, J., Qin, Y., Li, X., Parsawar, K., Larson, M.H., Cox, J., Cheng, Y., Lambowitz, A.M., Weissman, J.S., et al. (2015). Protein synthesis. Rqc2p and 60S ribosomal subunits mediate mRNA-independent elongation of nascent chains. Science *347*, 75–78. https://doi.org/10.1126/science.1259724.
15. Bengtson, M.H., and Joazeiro, C.A.P. (2010). Role of a ribosome-associated E3 ubiquitin ligase in protein quality control. Nature *467*, 470–473. https://doi.org/10.1038/nature09371.
16. Brandman, O., Stewart-Ornstein, J., Wong, D., Larson, A., Williams, C.C., Li, G.-W., Zhou, S., King, D., Shen, P.S., Weibezahn, J., et al. (2012). A Ribosome-Bound Quality Control Complex Triggers Degradation of Nascent Peptides and Signals Translation Stress. Cell *151*, 1042–1054. https://doi.org/10.1016/j.cell.2012.10.044.
17. Verma, R., Oania, R.S., Kolawa, N.J., and Deshaies, R.J. (2013). Cdc48/p97 promotes degradation of aberrant nascent polypeptides bound to the ribosome. eLife *2*, e00308. https://doi.org/10.7554/eLife.00308.
18. Defenouillère, Q., Zhang, E., Namane, A., Mouaikel, J., Jacquier, A., and Fromont-Racine, M. (2016). Rqc1 and Ltn1 Prevent C-terminal Alanine-Threonine Tail (CAT-tail)-induced Protein Aggregation by Efficient Recruitment of Cdc48 on Stalled 60S Subunits. J. Biol. Chem. *291*, 12245–12253. https://doi.org/10.1074/jbc.M116.722264.
19. Tesina, P., Ebine, S., Buschauer, R., Thoms, M., Matsuo, Y., Inada, T., and Beckmann, R. (2023). Molecular basis of eIF5A-dependent CAT tailing in eukaryotic ribosome-associated quality control. Mol. Cell *83*, 607–621.e4. https://doi.org/10.1016/j.molcel.2023.01.020.
20. Yonashiro, R., Tahara, E.B., Bengtson, M.H., Khokhrina, M., Lorenz, H., Chen, K.-C., Kigoshi-Tansho, Y., Savas, J.N., Yates, J.R., Kay, S.A., et al. (2016). The Rqc2/Tae2 subunit of the ribosome-associated quality control (RQC) complex marks ribosome-stalled nascent polypeptide chains for aggregation. eLife *5*, e11794. https://doi.org/10.7554/eLife.11794.
21. Osuna, B.A., Howard, C.J., Kc, S., Frost, A., and Weinberg, D.E. (2017). In vitro analysis of RQC activities provides insights into the mechanism and function of CAT tailing. eLife *6*, e27949. https://doi.org/10.7554/eLife.27949.
22. Kostova, K.K., Hickey, K.L., Osuna, B.A., Hussmann, J.A., Frost, A., Weinberg, D.E., and Weissman, J.S. (2017). CAT-tailing as a fail-safe mechanism for efficient degradation of stalled nascent polypeptides. Science *357*, 414–417. https://doi.org/10.1126/science.aam7787.
23. Svetlov, M.S., Dunand, C.F., Nakamoto, J.A., Atkinson, G.C., Safdari, H.A., Wilson, D.N., Vázquez-Laslop, N., and Mankin, A.S. (2024). Peptidyl-tRNA hydrolase is the nascent chain release factor in bacterial ribosome-associated quality control. Mol. Cell *84*, 715–726.e5. https://doi.org/10.1016/j.molcel.2023.12.002.
24. Sitron, C.S., and Brandman, O. (2019). CAT tails drive degradation of stalled polypeptides on and off the ribosome. Nat. Struct. Mol. Biol. *26*, 450–459. https://doi.org/10.1038/s41594-019-0230-1.
25. Lv, L., Mo, J., Qing, Y., Wang, S., Chen, L., Mei, A., Xu, R., Huang, H., Tan, J., Li, Y., et al. (2024). NEMF-mediated Listerin-independent mitochondrial translational surveillance by E3 ligase Pirh2 and mitochondrial protease ClpXP. Cell Rep. *43*, 113860. https://doi.org/10.1016/j.celrep.2024.113860.
26. Lytvynenko, I., Paternoga, H., Thrun, A., Balke, A., Müller, T.A., Chiang, C.H., Nagler, K., Tsaprailis, G., Anders, S., Bischofs, I., et al. (2019). Alanine

Tails Signal Proteolysis in Bacterial Ribosome-Associated Quality Control. Cell *178*, 76–90.e22. https://doi.org/10.1016/j.cell.2019.05.002.

27. Thrun, A., Garzia, A., Kigoshi-Tansho, Y., Patil, P.R., Umbaugh, C.S., Dallinger, T., Liu, J., Kreger, S., Patrizi, A., Cox, G.A., et al. (2021). Convergence of mammalian RQC and C-end rule proteolytic pathways via alanine tailing. Mol. Cell *81*, 2112–2122.e7. https://doi.org/10.1016/j.molcel.2021.03.004.

28. Choe, Y.-J., Park, S.-H., Hassemer, T., Körner, R., Vincenz-Donnelly, L., Hayer-Hartl, M., and Hartl, F.U. (2016). Failure of RQC machinery causes protein aggregation and proteotoxic stress. Nature *531*, 191–195. https://doi.org/10.1038/nature16973.

29. Izawa, T., Park, S.-H., Zhao, L., Hartl, F.U., and Neupert, W. (2017). Cytosolic Protein Vms1 Links Ribosome Quality Control to Mitochondrial and Cellular Homeostasis. Cell *171*, 890–903.e18. https://doi.org/10.1016/j.cell.2017.10.002.

30. Wu, Z., Tantray, I., Lim, J., Chen, S., Li, Y., Davis, Z., Sitron, C., Dong, J., Gispert, S., Auburger, G., et al. (2019). MISTERMINATE Mechanistically Links Mitochondrial Dysfunction with Proteostasis Failure. Mol. Cell *75*, 835–848.e8. https://doi.org/10.1016/j.molcel.2019.06.031.

31. Heo, J.-M., Livnat-Levanon, N., Taylor, E.B., Jones, K.T., Dephoure, N., Ring, J., Xie, J., Brodsky, J.L., Madeo, F., Gygi, S.P., et al. (2010). A stress-responsive system for mitochondrial protein degradation. Mol. Cell *40*, 465–480. https://doi.org/10.1016/j.molcel.2010.10.021.

32. Verma, R., Reichermeier, K.M., Burroughs, A.M., Oania, R.S., Reitsma, J.M., Aravind, L., and Deshaies, R.J. (2018). Vms1 and ANKZF1 peptidyl-tRNA hydrolases release nascent chains from stalled ribosomes. Nature *557*, 446–451. https://doi.org/10.1038/s41586-018-0022-5.

33. Kuroha, K., Zinoviev, A., Hellen, C.U.T., and Pestova, T.V. (2018). Release of Ubiquitinated and Non-ubiquitinated Nascent Chains from Stalled Mammalian Ribosomal Complexes by ANKZF1 and Ptrh1. Mol. Cell *72*, 286–302.e8. https://doi.org/10.1016/j.molcel.2018.08.022.

34. Su, T., Izawa, T., Thoms, M., Yamashita, Y., Cheng, J., Berninghausen, O., Hartl, F.U., Inada, T., Neupert, W., and Beckmann, R. (2019). Structure and function of Vms1 and Arb1 in RQC and mitochondrial proteome homeostasis. Nature *570*, 538–542. https://doi.org/10.1038/s41586-019-1307-z.

35. De Pereda, J.M., Waas, W.F., Jan, Y., Ruoslahti, E., Schimmel, P., and Pascual, J. (2004). Crystal structure of a human peptidyl-tRNA hydrolase reveals a new fold and suggests basis for a bifunctional activity. J. Biol. Chem. *279*, 8111–8115. https://doi.org/10.1074/jbc.M311449200.

36. Rosas-Sandoval, G., Ambrogelly, A., Rinehart, J., Wei, D., Cruz-Vera, L.R., Graham, D.E., Stetter, K.O., Guarneros, G., and Söll, D. (2002). Orthologs of a novel archaeal and of the bacterial peptidyl–tRNA hydrolase are nonessential in yeast. Proc. Natl. Acad. Sci. USA *99*, 16707–16712. https://doi.org/10.1073/pnas.222659199.

37. Schulte, U., den Brave, F., Haupt, A., Gupta, A., Song, J., Müller, C.S., Engelke, J., Mishra, S., Mårtensson, C., Ellenrieder, L., et al. (2023). Mitochondrial complexome reveals quality-control pathways of protein import. Nature *614*, 153–159. https://doi.org/10.1038/s41586-022-05641-w.

38. Sharkia, R., Jain, S., Mahajnah, M., Habib, C., Azem, A., Al-Shareef, W., and Zalan, A. (2023). PTRH2 Gene Variants: Recent Review of the Phenotypic Features and Their Bioinformatics Analysis. Genes *14*, 1031. https://doi.org/10.3390/genes14051031.

39. Ishii, T., Funakoshi, M., and Kobayashi, H. (2006). Yeast Pth2 is a UBL domain-binding protein that participates in the ubiquitin-proteasome pathway. EMBO J. *25*, 5492–5503. https://doi.org/10.1038/sj.emboj.7601418.

40. Joazeiro, C.A.P. (2017). Ribosomal Stalling During Translation: Providing Substrates for Ribosome-Associated Protein Quality Control. Annu. Rev. Cell Dev. Biol. *33*, 343–368. https://doi.org/10.1146/annurev-cellbio-111315-125249.

41. Chazotte, B. (2011). Labeling Mitochondria with MitoTracker Dyes. Cold Spring Harb. Protoc. *2011*, 990–992. https://doi.org/10.1101/pdb.prot5648.

42. Ito, Y., Chadani, Y., Niwa, T., Yamakawa, A., Machida, K., Imataka, H., and Taguchi, H. (2022). Nascent peptide-induced translation discontinuation in eukaryotes impacts biased amino acid usage in proteomes. Nat. Commun. *13*, 7451. https://doi.org/10.1038/s41467-022-35156-x.

43. Chang, W.D., Yoon, M.-J., Yeo, K.H., and Choe, Y.-J. (2024). Threonine-rich carboxyl-terminal extension drives aggregation of stalled polypeptides. Mol. Cell *84*, 4334–4349.e7. https://doi.org/10.1016/j.molcel.2024.10.011.

44. Stan, T., Ahting, U., Dembowski, M., Künkele, K.P., Nussberger, S., Neupert, W., and Rapaport, D. (2000). Recognition of preproteins by the isolated TOM complex of mitochondria. EMBO J. *19*, 4895–4902. https://doi.org/10.1093/emboj/19.18.4895.

45. Genge, M.G., Roy Chowdhury, S., Dohnálek, V., Yunoki, K., Hirashima, T., Endo, T., Doležal, P., and Mokranjac, D. (2023). Two domains of Tim50 coordinate translocation of proteins across the two mitochondrial membranes. Life Sci. Alliance *6*, e202302122. https://doi.org/10.26508/lsa.202302122.

46. Banerjee, R., Gladkova, C., Mapa, K., Witte, G., and Mokranjac, D. (2015). Protein translocation channel of mitochondrial inner membrane and matrix-exposed import motor communicate via two-domain coupling protein. eLife *4*, e11897. https://doi.org/10.7554/eLife.11897.

47. Wagener, N., Ackermann, M., Funes, S., and Neupert, W. (2011). A pathway of protein translocation in mitochondria mediated by the AAA-ATPase Bcs1. Mol. Cell *44*, 191–202. https://doi.org/10.1016/j.molcel.2011.07.036.

48. Jores, T., Lawatscheck, J., Beke, V., Franz-Wachtel, M., Yunoki, K., Fitzgerald, J.C., Macek, B., Endo, T., Kalbacher, H., Buchner, J., et al. (2018). Cytosolic Hsp70 and Hsp40 chaperones enable the biogenesis of mitochondrial β-barrel proteins. J. Cell Biol. *217*, 3091–3108. https://doi.org/10.1083/jcb.201712029.

49. Janke, C., Magiera, M.M., Rathfelder, N., Taxis, C., Reber, S., Maekawa, H., Moreno-Borchart, A., Doenges, G., Schwob, E., Schiebel, E., et al. (2004). A versatile toolbox for PCR-based tagging of yeast genes: new fluorescent proteins, more markers and promoter substitution cassettes. Yeast *21*, 947–962. https://doi.org/10.1002/yea.1142.

50. Houseley, J., and Tollervey, D. (2011). Repeat expansion in the budding yeast ribosomal DNA can occur independently of the canonical homologous recombination machinery. Nucleic Acids Res. *39*, 8778–8791. https://doi.org/10.1093/nar/gkr589.

51. Longtine, M.S., McKenzie, A., Demarini, D.J., Shah, N.G., Wach, A., Brachat, A., Philippsen, P., and Pringle, J.R. (1998). Additional modules for versatile and economical PCR-based gene deletion and modification in Saccharomyces cerevisiae. Yeast *14*, 953–961. https://doi.org/10.1002/(SICI)1097-0061(199807)14:10<953::AID-YEA293>3.0.CO;2-U.

52. Popov-Čeleketić, D., Waegemann, K., Mapa, K., Neupert, W., and Mokranjac, D. (2011). Role of the import motor in insertion of transmembrane segments by the mitochondrial TIM23 complex. EMBO Rep. *12*, 542–548. https://doi.org/10.1038/embor.2011.72.

53. Schindelin, J., Arganda-Carreras, I., Frise, E., Kaynig, V., Longair, M., Pietzsch, T., Preibisch, S., Rueden, C., Saalfeld, S., Schmid, B., et al. (2012). Fiji: an open-source platform for biological-image analysis. Nat. Methods *9*, 676–682. https://doi.org/10.1038/nmeth.2019.

54. Cox, J., and Mann, M. (2008). MaxQuant enables high peptide identification rates, individualized p.p.b.-range mass accuracies and proteome-wide protein quantification. Nat. Biotechnol. *26*, 1367–1372. https://doi.org/10.1038/nbt.1511.

55. Tyanova, S., Temu, T., and Cox, J. (2016). The MaxQuant computational platform for mass spectrometry-based shotgun proteomics. Nat. Protoc. *11*, 2301–2319. https://doi.org/10.1038/nprot.2016.136.

56. Hallgren, J., Tsirigos, K.D., Pedersen, M.D., Almagro Armenteros, J.J.A., Marcatili, P., Nielsen, H., Krogh, A., and Winther, O. (2022). DeepTMHMM predicts alpha and beta transmembrane proteins using deep neural networks. Preprint at bioRxiv. https://doi.org/10.1101/2022.04.08.487609.

57. Schrott, S., and Osman, C. (2023). Two mitochondrial HMG-box proteins, Cim1 and Abf2, antagonistically regulate mtDNA copy number in Saccharomyces cerevisiae. Nucleic Acids Res. *51*, 11813–11835. https://doi.org/10.1093/nar/gkad849.

58. Schreiner, B., Westerburg, H., Forné, I., Imhof, A., Neupert, W., and Mokranjac, D. (2012). Role of the AAA protease Yme1 in folding of proteins in the intermembrane space of mitochondria. Mol. Biol. Cell *23*, 4335–4346. https://doi.org/10.1091/mbc.E12-05-0420.

59. Tong, A.H.Y., and Boone, C. (2007). 16 High-Throughput Strain Construction and Systematic Synthetic Lethal Screening in Saccharomyces cerevisiae. In Methods in Microbiology Yeast Gene Analysis, I. Stansfield and M.J. Stark, eds. (Academic Press), pp. 369–707. https://doi.org/10.1016/S0580-9517(06)36016-3.

60. Tong, A.H., Evangelista, M., Parsons, A.B., Xu, H., Bader, G.D., Pagé, N., Robinson, M., Raghibizadeh, S., Hogue, C.W., Bussey, H., et al. (2001). Systematic genetic analysis with ordered arrays of yeast deletion mutants. Science *294*, 2364–2368. https://doi.org/10.1126/science.1065810.

61. Scherzinger, E., Lurz, R., Turmaine, M., Mangiarini, L., Hollenbach, B., Hasenbank, R., Bates, G.P., Davies, S.W., Lehrach, H., and Wanker, E. E. (1997). Huntingtin-Encoded Polyglutamine Expansions Form Amyloid-like Protein Aggregates In Vitro and In Vivo. Cell *90*, 549–558. https://doi.org/10.1016/S0092-8674(00)80514-0.

62. Bouchez, C.L., Hammad, N., Cuvellier, S., Ransac, S., Rigoulet, M., and Devin, A. (2020). The Warburg Effect in Yeast: Repression of Mitochondrial Metabolism Is Not a Prerequisite to Promote Cell Proliferation. Front. Oncol. *10*, 1333. https://doi.org/10.3389/fonc.2020.01333.

63. Rappsilber, J., Ishihama, Y., and Mann, M. (2003). Stop and go extraction tips for matrix-assisted laser desorption/ionization, nanoelectrospray, and LC/MS sample pretreatment in proteomics. Anal. Chem. *75*, 663–670. https://doi.org/10.1021/ac026117i.

64. Espinoza-Corral, R., Schwenkert, S., and Schneider, A. (2023). Characterization of the preferred cation cofactors of chloroplast protein kinases in Arabidopsis thaliana. FEBS Open Bio *13*, 511–518. https://doi.org/10.1002/2211-5463.13563.

65. Cox, J., Hein, M.Y., Luber, C.A., Paron, I., Nagaraj, N., and Mann, M. (2014). Accurate proteome-wide label-free quantification by delayed normalization and maximal peptide ratio extraction, termed MaxLFQ. Mol. Cell. Proteomics *13*, 2513–2526. https://doi.org/10.1074/mcp.M113.031591.

66. RStudio Team (2019). RStudio: Integrated Developement for R, Version 1.2.5001 (RStudio, Inc.).

67. Bolte, S., and Cordelières, F.P. (2006). A guided tour into subcellular colocalization analysis in light microscopy. J. Microsc. *224*, 213–232. https://doi.org/10.1111/j.1365-2818.2006.01706.x.

68. Lord, S.J., Velle, K.B., Mullins, R.D., and Fritz-Laylin, L.K. (2020). SuperPlots: Communicating reproducibility and variability in cell biology. J. Cell Biol. *219*, e202001064. https://doi.org/10.1083/jcb.202001064.

STAR★METHODS

KEY RESOURCES TABLE

REAGENT or RESOURCE	SOURCE	IDENTIFIER
Antibodies		
Rabbit anti-Pth2	This study	Pth2, Rabbit 3, affinity purified
Mouse monoclonal anti-GFP	Roche	Cat. #11814460001; RRID:AB_390913
Rabbit anti-Tom70	Stan et al.[44]	Rabbit 312
Rabbit anti-Tom40	Genge et al.[45]	Rabbit 547, affinity purified
Rabbit anti-Tim23C-term	Neupert lab antibodies	Tim23C-pep, affinity purified
Rabbit anti-Tim44	Banjeree et al.[46]	Rabbit 388, affinity purified
Rabbit anti-Rip1	Wagener et al.[47]	Rip1C-pep, affinity purified
Rabbit anti-Ssq1	Izawa et al.[29]	N/A
Mouse monoclonal anti-Pgk1	Life Technologies	Cat. #459250
Rabbit anti-F1ß	Izawa et al.[29]	Rabbit 421
Rabbit anti-Porin	Neupert lab antibodies	Rabbit 87118
Rabbit anti-Sis1	Jores et al.[48]	N/A
Goat Anti-Mouse IgG (H+L)-HRP Conjugate	Bio-Rad	Cat. #1706516; RRID:AB_11125547
Goat Anti-Rabbit IgG (H+L)-HRP Conjugate	Bio-Rad	Cat. #1706515, RRID:AB_11125142
Chemicals, peptides, and recombinant proteins		
5-Fluoroorotic acid (5-FOA)	US Biological Life Sciences	Cat. #F5050
Bacto Peptone Gibco	Otto Nordwald	Cat. #211830
Bacto yeast Extract	Otto Nordwald	Cat. #212730
Yeast Nitrogen Base	Otto Nordwald	Cat. #291920
(S)-Lactic acid	MERCK	Cat. # 100366
Trichloroacetic acid (TCA)	Sigma-Aldrich	Cat. #T6399
Triton X-100	VWR	Cat. #M143
Digitonin	Calbiochem	Cat. # 300410
D(+)-Galactose	Sigma-aldrich	Cat. #48260
D(+)-Glucose	VWR	Cat. #24371.366
Glycerol	VWR	Cat. #24387.361
VeriFi® Polymerase	PCRBiosystems	Cat. #PB10.42-01
highQu ALLin™ Hifi DNA Polymerase	HighQu	Cat. # HLE0201
RibonucleaseA	ROTH	Cat. #9001-99-4
ChromoTek GFP-Trap® Magnetic Particles M-270	Proteintech	Cat. #AB_2827592
Sodium carbonate (Na_2CO_3)	ROTH	Cat. #P028-1
Glass beads 0.25–0.5 mm	ROTH	Cat. #A553.1
Urea	ROTH	Cat. #57-13-6
Phenylmethylsulfonylfluorid (PMSF)	Serva	Cat. #32395.04
DL-Dithiothreitol (DTT)	Sigma-Aldrich	Cat. #43819
Dodecylsulfate-Na-salt (SDS)	Serva	Cat. #20765.03
Trizma® base (TRIS)	Sigma-Aldrich	Cat. #T1503-25G
2-Mercaptoethanol	Sigma-Aldrich	Cat. #M3148
Complete protease inhibitor cocktail, EDTA-free	Roche	Cat. #05 056 489 001
Deposited data		
Raw mass spectrometry data	This study	PRIDE: PXD057575

(*Continued on next page*)

Continued

REAGENT or RESOURCE	SOURCE	IDENTIFIER
Raw microscopy and picture data	This study	Mendeley Data: https://doi.org/10.17632/5vywz7sv39.1
Experimental models: Organisms/strains		
BY4742	EUROSCARF	Y10000
BY4742 *vms1Δ::kanMX4*	Izawa et al.[29]	N/A
BY4742 *ltn1Δ::kanMX4*	Izawa et al.[29]	N/A
BY4742 *pth2Δ::HIS3MX6*	This study	N/A
BY4742 *pth1Δ*::natNT2	This study	N/A
BY4742 *pth2Δ::HIS3MX6 pth1Δ::natNT2*	This study	N/A
BY4742 *vms1Δ::HIS3MX6 ltn1Δ::kanMX4*	Izawa et al.[29]	N/A
BY4742 *vms1Δ::kanMX4 pth2Δ::LEU2*	This study	N/A
BY4742 *ltn1Δ::kanMX4 pth2Δ::HIS3MX6*	This study	N/A
BY4742 *vms1Δ::HIS3MX6 ltn1Δ::kanMX4 rqc2Δ::LEU2*	Izawa et al.[29]	N/A
BY4742 *vms1Δ::HIS3MX6 ltn1Δ::kanMX4 pth2Δ::LEU2*	This study	N/A
BY4742 *vms1Δ::HIS3MX6 ltn1Δ::kanMX4 pth1Δ::natNT2*	This study	N/A
BY4742 *vms1Δ::HIS3MX6 ltn1Δ::kanMX4 tom6Δ::LEU2*	This study	N/A
BY4742 *vms1Δ::HIS3MX6 ltn1Δ::kanMX4 tim21Δ::LEU2*	This study	N/A
BY4742 *vms1Δ::HIS3MX6 ltn1Δ::kanMX4 pth2Δ::LEU2 + LEU2::Pth2*	This study	N/A
BY4742 *vms1Δ::HIS3MX6 ltn1Δ::kanMX4 pth2Δ::LEU2 + LEU2::Pth2N-GFP*	This study	N/A
BY4742 *vms1Δ::HIS3MX6 ltn1Δ::kanMX4 pth2Δ::LEU2 + LEU2::TM$_{Tom70}$-Pth2*	This study	N/A
BY4742 *vms1Δ::HIS3MX6 ltn1Δ::kanMX4 pth2Δ::LEU2 + LEU2::Pth2$^{\Delta TM}$*	This study	N/A
BY4742 *vms1Δ::HIS3MX6 ltn1Δ::kanMX4 pth2Δ::LEU2 + LEU2::Pth2^{D174N}*	This study	N/A
BY4742 *vms1Δ::HIS3MX6 ltn1Δ::kanMX4 pth2Δ::LEU2 + LEU2::Pth2N-Pth1*	This study	N/A
BY4742 *vms1Δ::HIS3MX6 ltn1Δ::kanMX4 pth2Δ::LEU2 + LEU2::Pth2N-Pth1^{H24N}*	This study	N/A
BY4742 +p426_Gal1_NS-mtGFP	This study	N/A
BY4742 *vms1Δ::kanMX4* +p426_Gal1_NS-mtGFP	This study	N/A
BY4742 *ltn1Δ::kanMX4* +p426_Gal1_NS-mtGFP	This study	N/A
BY4742 *pth2Δ::HIS3MX6* +p426_Gal1_NS-mtGFP	This study	N/A
BY4742 *vms1Δ*::kanMX4 *pth2Δ*::LEU2 +p426_Gal1_NS-mtGFP	This study	N/A
BY4742 ltn1*Δ::kanMX4 pth2Δ::HIS3MX6* +p426_Gal1_NS-mtGFP	This study	N/A
BY4742 *vms1Δ::HIS3MX6 ltn1Δ::kanMX4* +p426_Gal1_NS-mtGFP	This study	N/A
BY4742 *vms1Δ::HIS3MX6 ltn1Δ::kanMX4 pth2Δ::LEU2* +p426_Gal1_NS-mtGFP	This study	N/A
BY4742 *vms1Δ::HIS3MX6 ltn1Δ::kanMX4 rqc2Δ::LEU2* +p426_Gal1_NS-mtGFP	This study	N/A

(*Continued on next page*)

Continued

REAGENT or RESOURCE	SOURCE	IDENTIFIER
D273-10b	Neupert Lab strain collection	N/A
BY4742 Pth1-yEGFP	This study	N/A
BY4742 +pYes2	This study	N/A
BY4742 +mtGFP$_{AT10}$	This study	N/A
BY4742 +mtGFP$_{AT15}$	This study	N/A
Oligonucleotides		
Primers for cloning (see Table S3)	This study	N/A
Recombinant DNA		
pSS036_Pth2_500bp	This study	N/A
pSS036_TM$_{Tom70}$-Pth2_500bp	This study	N/A
pSS036_Pth2N-GFP_500bp	This study	N/A
pSS036_Pth2$^{\Delta TM}$_500bp	This study	N/A
pSS036_Pth2^{D174N}_500bp	This study	N/A
pSS036_Pth2N-Pth1_500bp	This study	N/A
pSS036_Pth2N-Pth1^{H24N}_500bp	This study	N/A
p416_Gal1_NS-mtGFP	Izawa et al.[29]	N/A
p426_Gal1_NS-mtGFP	This study	N/A
pYM25	Janke et al.[49]	P30237
pFA6a_natNT2	Janke et al.[49]	P30346
pFA6a_LEU2	Houseley and Tollervey[50]	#61923
pFA6a_His3MX6	Longtine et al.[51]	#41596
pYes2	Popov-Celeketic et al.[52]	Cat. #V82520
pYes2-mtGFP$_{AT10}$	This study	N/A
pYes2-mtGFP$_{AT15}$	This study	N/A
Software and algorithms		
ImageJ 1.54p	Schindelin et al.[53]	RRID:SCR_003070
R-studio	RStudio Team (2020)	N/A
MaxQuant 2.4.4.0	Cox and Mann[54]	N/A
Perseus version 2.0.9.0	Tyanova et al.[55]	N/A
Affinity Designer 1.10.6	https://affinity.serif.com/de/designer	N/A
SPECTROstar©Nano 5.70 R2	BMG Labtech	N/A
SPECTROstar©Nano MARS 4.01 R2	BMG Labtech	N/A
DeepTMHMM - 1.0	Hallgren et al.[56]	RRID:SCR_025039
Jupyter Notebook 6.4.12	https://jupyter-notebook.readthedocs.io/en/6.4.12/	N/A
NIS-ELEMENTS AR 5.21.03	https://www.nisoftware.net/NikonSaleApplication/Default.aspx	N/A
Huygens essential 21.10.0p0 64b	https://svi.nl/Huygens-Essential	N/A
Other		
NuPAGE™ 4-12% Bis-Tris-Gel	Thermo Fisher Scientific	Cat. #NP0322BOX
NativePAGE™ 3-12% Bis-Tris-Gel	Thermo Fisher Scientific	Cat. #BN1001BOX
Cellulose Acetate Membrane Circle (OE 66)	GE Healthcare	Cat. #10404131

EXPERIMENTAL MODEL AND STUDY PARTICIPANT DETAILS

Yeast strains and plasmids

The wild-type *Saccharomyces cerevisiae* strain BY4742 (*Mat α his3Δ1 leu2Δ0 lys2Δ0 ura3Δ0*) was used for all genetic manipulations. A comprehensive list of yeast strains and plasmids can be found in STAR Methods key resource table and of primers in Table S3.

Chromosomal tagging and deletions were made by homologous recombination of PCR products, as described previously.[49] The junctions were all confirmed by PCR and, if possible, also on protein level.

The various Pth2 constructs were genomically integrated into the *LEU* locus in a markerless manner, as described previously.[57] Briefly, DNA sequence encoding *PTH2*, together with ca. 500bp upstream and downstream of the ORF, was amplified from yeast genomic DNA and cloned into pSS036[57] via Gibson assembly, exchanging the DNA sequence encoding mitochondrially targeted mKate2 under the control of the *PGK1* promoter and the *ADH1* terminator with the *PTH2* sequence along with its promoter and 3'UTR. This plasmid served as a template for generation of all different Pth2 constructs using either Gibson assembly or mutagenesis PCRs. Before transformation into yeast, the plasmids were digested with NotI and transformants initially selected on selective glucose medium lacking uracil and subsequently on medium containing 5-FOA to remove the *URA* marker by recombination.[57]

The construct p426Gal1-NS-mtGFP was created by digesting p416Gal1-NS-mtGFP[29] with SacI and EcoRI and subcloning the fragment into SacI/EcoRI digested pRS426.

pYES2-mtGFP$_{AT10}$ was generated by inserting the EcoRI/BamHI-digested GFP fragment from p416GAL1-mtGFP-(AT)$_{10}$[29] into EcoRI/BamHI-digested pYES2, followed by addition of the matrix-targeting signal of yeast cytochrome b_2 (b_2(1–107)Δ19) as a HindIII/BamHI fragment cut out from pYes2-b$_2$(1-107)Δ19-DHFRmut.[58] pYES2-mtGFP$_{AT15}$ was subsequently created from pYES2-mtGFP$_{AT10}$ by mutagenesis PCR.

All plasmids were confirmed by Sanger sequencing.

Yeast cells were typically grown at 30°C in YP medium (10 g/L yeast extract, 20 g/L bactopeptone, pH 5.5) containing 2% of either glucose (YPD), galactose (YPGal), or glycerol (YPG), as a carbon source or in selective medium (1.7 g/L yeast nitrogen base, 5 g/L $(NH_4)_2SO_4$, 0.02 mg/mL adenine, 0.02 mg/mL histidine, 0.03 mg/mL leucine, 0.03 mg/mL lysine, 0.004 mg/mL tryptophan, pH 5.5) containing either 2% glucose (SD) or 2% lactate (SLac) as a carbon source.

Mitochondria were isolated from BY4742 Pth1-yEGFP and D273-10b cells grown in Lactate medium (3 g yeast extract, 1 g KH_2PO_4, 1 g NH_4Cl, 0.5 g $CaCl_2$x2H_2O, 0.5 g NaCl, 1.1 g $MgSO_4$x6H_2O, 0.3 ml 1% $FeCl_3$, 22 ml of 90 % lactic acid, dH_2O to 1 L, pH 5.5, supplemented with 0.1 % glucose) at 30°C, and BY4742, BY4742 *Δvms1Δltn1*, BY4742 *Δvms1Δltn1Δpth2* and BY4742 *Δvms1Δltn1Δrqc2* grown in YPGal 37°C, as described in Genge et al. (2023).[45]

METHOD DETAILS

Synthetic genetic array analysis

Synthetic genetic array analysis was performed essentially as described in Tong and Boone (2007).[59] Briefly, the MATa strain carrying query mutations (*Δvms1::natNT2*, *Δltn1::hphNT1*) was constructed from the parental strain Y8205 (*MATα Δcan1::STE2pr-his5 Δlyp1::STE3pr-LEU2 ura3Δ0 leu2Δ0 his3Δ1 met15Δ0*)[60] and mated with the deletion mutant library (Thermo Fisher) using Biomek FXP (Beckman Coulter). After selection of diploid cells, sporulation was induced by transferring cells to sporulation medium containing 1% potassium acetate. The triple deletion mutants carrying *Δvms1::natNT2*, *Δltn1::hphNT1 and XXXΔ::kanMX4* were selected by transferring cells to the plates containing nourseothricin, hygromycin B and G418. The strains were then spotted onto the YPG plates, grown at 37°C for 3 days and their growth areas were measured. Each strain was generated in duplicates. Deletions with a z-score higher than 4.0 in both replicates are listed in Table S1.

Analysis of growth of yeast cells

Growth of yeast cells was analyzed either by serial dilution spot assay on plates or in liquid media. For growth analysis on plates, yeast cells were grown in liquid YPD medium or in selective lactate medium containing 0.1% glucose ON at 30°C. ON cultures were diluted into fresh medium and grown until OD ca. 0.5. One OD of cells were then transferred into sterile tubes, cells were pelleted by centrifugation (16000 rcf, 2 min, RT) and resuspended in 1mL sterile dH_2O. Subsequently, four ten-fold serial dilutions were made in sterile dH_2O and 2 µl of cell suspensions were spotted on plates. The plates were incubated at indicated temperatures for 2 to 3 days.

Growth of yeast cells in liquid medium was analysed in 96-well plates using the SPECTROstar Nano (BMG Labtech). To this end, ON cultures were diluted into fresh medium and grown till OD ca. 0.5. The cells were then collected, washed three times with sterile ddH_2O, resuspended in YPG medium to an OD_{600} of 0.1 and aliquoted into wells of a 96-well plate. Growth at 30°C was monitored every 20 minutes for up to 72h under constant shaking at 800 rpm. All growth curves shown represent the mean of three biological replicates, each comprising technical triplicates. Calculations and visualizations were carried out using the SPECTROstar©Nano MARS 4.01 R2 software and Excel.

Submitochondrial localization

Isolated mitochondria were resuspended in either SH buffer (0.6 M sorbitol, 20 mM HEPES/KOH, pH 7.4), to keep mitochondria intact, in 20 mM HEPES/KOH, pH 7.4, to burst the outer membrane and generate mitoplasts, or in 20 mM HEPES/KOH, pH 7.4 containing 0.25% Triton X-100, to solubilize mitochondrial membranes. Where indicated, proteinase K was added and the samples were incubated for 20min on ice. PMSF (1 mM) was then added to inhibit the protease and the samples were further incubated for 5 min on ice. Mitochondria and mitoplasts were reisolated by centrifugation (18000 rcf, 10 min, 4°C), resuspended in 2x Laemmli buffer (120mM Tris/HCl, pH 6.8, 20% glycerol, 4% SDS, 0.02% bromphenol blue, 3% ß-mercaptoethanol), incubated for 5 min at 95°C and then stored at -20°C until SDS-PAGE analysis. Triton X-100-solubilized sample was TCA-precipitated before resuspension in 2x Laemmli buffer and analysis by SDS-PAGE and western blot.

To analyze membrane association of proteins by carbonate extraction, isolated mitochondria were incubated in 100 mM freshly prepared Na_2CO_3 for 30 min on a rotating platform at 4°C. One aliquot was taken as total and TCA-precipitated. The rest of the sample was centrifuged (30 min, 186000 rcf, 2°C) and thereby separated into the supernatant fraction, which contains the soluble and peripheral membrane proteins, and the pellet fraction which contains integral membrane proteins. The pellet fraction was directly resuspended in 2x Laemmli buffer whereas the supernatant was first TCA-precipitated. All samples were analyzed by SDS-PAGE and western blot.

Total cell extracts

Total cell extracts for analysis of CAT-tail proteins were prepared essentially as described in Izawa et al. (2017).[29] Briefly, expression of NS-mtGFP from the p426*GAL1*-NS-mtGFP plasmid was induced by addition of 0.5% galactose for 20h to logarithmically growing cells in selective lactate medium at 30°C. Cells (3 OD_{600}) were harvested by centrifugation (5000 rcf, 5 min, RT) and resuspended in 1 mL ice-cold H_2O before 150 µl of solution containing 2 M NaOH and 7 % ß-mercaptoethanol were added. After 10 min incubation on ice, TCA was added to 12% final concentration and samples were incubated for an additional 30 min on ice. The precipitated proteins were isolated by centrifugation (17000 rcf, 10min, 2°C), washed with 1 mL ice-cold acetone and the final pellet was resuspended in 80 µl HU-buffer, incubated for 5 min at 95°C and analyzed by SDS-PAGE (1.5 OD_{600} per lane) followed by western blot.

Protein aggregation assay

Endogenous protein aggregates were isolated essentially as previously described in Izawa et al. (2017).[29] Briefly, yeast cells were grown in YPGal medium ON at 37°C and diluted the next day into fresh medium. When the cultures reached OD ca. 0.5, 35 OD_{600} of cells were collected by centrifugation (3220 rcf, 5min, RT), the pellets were resuspended in 500 µl IP buffer (50 mM Tris/HCl pH 7.4, 20 mM KCl, 10 mM $MgCl_2$, 1mM PMSF, Protease inhibitor cocktail) and 100 µl glass beads were added. Cells were lysed by vortexing four times for 30s, with 30s pauses on ice in between, the samples were diluted with 500 µl IP buffer containing 1 % Triton X-100 and incubated for 10 min at 4°C with gentle rolling. After removal of the cell debris by centrifugation (840 rcf, 10min, 2°C), an aliquot corresponding to 5 OD_{600} was taken as total (T) and the rest of the lysates were separated into soluble (S) and pellet (P) material by centrifugation (20000 rcf, 15min, 2°C). The pellets, containing aggregated proteins, were resolved in HU buffer (8 M urea, 5% SDS, 200 mM Tris/HCl pH 6.8, 1mM EDTA, 0.01% bromophenol blue, 2% ß-mercaptoethanol), incubated for 5 min at 95°C and stored at -20°C until loading on SDS-PA gels. Proteins in T and S fractions were first TCA-precipitated (12% TCA), resolved in HU buffer, incubated for 5 min at 95°C and analyzed, together with the aggregate fraction, by SDS-PAGE followed by western blot. The material corresponding to 6 OD_{600} was loaded per lane for P and 0.6 OD_{600} per lane for T and S fractions.

Filter trap assay

Analysis of insoluble protein aggregates was performed as previously described (Izawa et al., 2017).[29] A total of 180 OD_{600} of cells expressing NS-mtGFP for 20 hours were harvested and lysed in 1.2 mL of lysis buffer (25 mM Tris/HCl, pH 7.5, 50 mM KCl, 10 mM $MgCl_2$, 1 mM EDTA, 5% glycerol, 1x protease inhibitor tablet (Roche)) using a FastPrep-24 homogenizer equipped with a CoolPrep adaptor (MP Biomedicals). Lysates were clarified by centrifugation at 1,000 rcf for 10 minutes at 4 °C. Protein concentration in the lysates was determined using BCA assay (Bio-Rad) and specified amounts of proteins were either mixed 1:1 with 4% SDS, 100 mM DTT or with lysis buffer. SDS/DTT-treated samples were boiled at 95 °C for 3 minutes. All samples were then filtered through a 0.2 µm cellulose acetate membrane using a dot blot apparatus (Scherzinger et al., 1997).[61] Membranes were immunodecorated with an anti-GFP antibody and visualized using HRP-labelled secondary antibodies and chemiluminescence. The signal intensities obtained with 200 µg SDS-treated samples were quantified using a standardized box and the "mean intensity" measurement functions in Fiji. Four biological replicates, each containing one replicate detected with the ImageQuant LAS 4000 mini (GE Healthcare) and one with Super RX X-ray film (Fujifilm), were analyzed. Mean values for each replicate were compared using a Student's t-test function in Excel.

Blue Native-PAGE

Isolated mitochondria (5 mg/mL) were solubilized with 1.5 % digitonin in 50 mM NaCl, 50 mM imidazole, 1 mM EDTA, 1 mM PMSF, pH 7.0 on a rotating platform at 4°C for 10 min. Insoluble material was removed by centrifugation (150000 rcf, 15 min, 4°C), sample additive (ThermoFisher) and glycerol were added to the clarified extracts and samples were separated on 3-12% Native gels (ThermoFisher) according to the manufacturer's instructions. Gels were subsequently blotted on PVDF membranes and the membranes decorated with the indicated antibodies.

Oxygen consumption assay

Oxygen consumption was measured polarographically at 28°C using a Clark oxygen electrode (Chauvin-Arnoux) in a 1 mL thermostatically controlled chamber essentially as described before.[62] Briefly, yeast cells were grown in YPGal medium at 37°C. Glycerol (10% (v/v)) was added to cultures in logarithmic growth phase, the cultures were frozen and kept at -80°C until use. Cells were thawed, washed, resuspended in fresh medium and transferred to the chamber (3-6 OD/mL). Respiratory rates were determined from the slope of O_2 concentration decrease over time. Measured activities were normalized per optical density unit at 600 nm and expressed in nano-atoms of Oxygen per minute and OD. Spontaneous respiratory rates were determined after addition of

100 mM ethanol. Uncoupled respiratory rates were measured after addition of 10 μM CCCP. Graphs show the means of four independent replicate measurements for the respective strains. Calculations and visualizations were performed in Excel.

Determination of enzymatic activities

Cells, as detailed for oxygen consumption assay, were resuspended in 50 mM Tris/HCl pH 7.5, and broken by vigorous shaking (FastPrep MP Biomedicals, 4 m/s, 5 cycles 20s, 5min on ice in between) with an equal volume of glass beads. Unbroken cells and glass beads were removed by centrifugation. Protein concentration in cellular extracts was determined using the BCA (bicinchoninic acid) method (Pierce BCA Protein assay kit). Citrate synthase (EC2.3.3.1) activity was determined by monitoring the formation of coenzyme A, produced by citrate synthase from acetyl-CoA and oxaloacetate, by spectrophotometrically measuring the free sulfhydryl groups using Ellman's reagent 5,5'-dithiobis-2-nitrobenzoic acid (DTNB) over time at 412 nm, in a spectrophotometer (SAFAS, Monaco).[62] Activity measurements were started by adding 10-100 μL of cellular extract to 50 mM Tris/HCl buffer pH 7.5 containing 0.05 % Triton-X100, 0.5 mM oxaloacetate, 0.1 mM acetyl-CoA, and 0.2 mM DTNB. When the signal increased linearly, the enzyme activity was calculated from the slope using an extinction coefficient of 13600 $M^{-1}cm^{-1}$ and expressed in nmoles of DTNB reduced per minute and mg protein. Cytochrome c oxidase activity (EC7.1.1.9; 5 mM potassium cyanide-sensitive) was determined by spectrophotometrically (550 nm) monitoring the rate of disappearance of reduced cytochrome c in the following buffer: 50 mM K-phosphate buffer, pH 7.5, 25 μM reduced cytochrome c.[62] The assay was started by adding 10-40 μL of cellular extract. The enzyme activity was determined using an extinction coefficient of 18500 $M^{-1}cm^{-1}$ and expressed in nmoles of cytochrome c per minute and mg protein. Results shown are means of multiple measurements (5 to 12) from two to four separate samples. Calculations and visualizations were performed in Excel.

Peptidyl-tRNA accumulation assay

To assess the presence of peptidyl-tRNAs in cells, the protocol described in Verma et al. (2013)[17] was modified. Briefly, yeast cells (5 OD_{600}) were washed three times with 1 mL ice cold buffer containing 50 mM Tris/HCl, pH7.5, 10 mM NaN_3, 10 mM EDTA, 10 mM EGTA, 1x protease inhibitor tablet (Roche), 10 mM NEM, 50 mM NaF, 60 mM ß-glycerophosphate, 10 mM sodium pyrophosphate, and split into two 200 μl aliquots. The cells were reisolated and 50 μl glass beads were added together with 40 μl SDS buffer (120 mM MOPS/NaOH, pH 6.8, 20 % glycerol, 4 % SDS, 0.02 % bromphenol blue) containing either 1 % DEPC and 2 % ß-mercaptoethanol or 200 ng/μl RibonucleaseA. Cells were incubated at 65°C for 5 min and vigorously vortexed for 1 min. ß-mercaptoethanol was added to 2% to RNaseA-treated samples. All samples were incubated for 3 min at 95°C, centrifuged for 1 min at 16000 rcf and directly loaded on 4-12 % NuPAGE gels (Thermo fisher). Gels were run in MOPS buffer (Thermo fisher) according to manufacturer's instructions and subsequently blotted on nitrocellulose membranes.

Immunoprecipitation of NS-mtGFP

Cells (180 OD_{600}), 20h after expression of NS-mtGFP was induced, were collected by centrifugation (3220 rcf, 5min, RT) and resuspended in 600 μl lysis buffer (25 mM Tris/HCl, pH 7.5, 50 mM KCl, 10 mM $MgCl_2$, 1 mM EDTA, 5% glycerol, 1x protease inhibitor tablet (Roche)). Glass beads (50 μl) were added and the cells were vortexed four times for 30s with 30s pauses on ice. The samples were diluted with 600 μl lysis buffer containing 1% Triton X-100 and incubated for 10 min on a rolling platform at 4°C. After a clarifying spin (1000 rcf, 10 min, 4°C), 1 mL of lysate was added to 10 μl GFP-Trap® Magnetic Particles M-270 (Chromotek/ Proteintech) and incubated for 2h at 4°C on a rotating platform. During this time, the remaining lysate was diluted with ice cold water to 1 mL and the proteins therein TCA-precipitated (12% TCA). GFP-Trap beads were isolated using a magnetic rack, the non-bound fraction was removed and the beads were subsequently washed three times for 10 min with 500 μl lysis buffer containing 0.05% Triton X-100. The specifically bound proteins were either directly eluted with HU buffer and incubation for 5 min at 95°C for analysis by SDS-PAGE and western blot or were directly used for on bead digest and mass spectrometry.

For mass spectrometry, three biological replicates of each strain were analyzed. The beads were washed twice with 50 mM Tris/HCl, pH 7.5, and subsequently with 50 mM Tris/HCl, pH 7.5 containing 2 M urea. For the first trypsin digest, the beads were resuspended in 160 μl of 50 mM Tris/HCl, pH 7.5, 1 M urea, 1 mM Dithiothreitol (DTT), and 0.8 μg of trypsin (Pierce, Thermo Scientific) were added and incubated for 3 h at 25°C with continuous shaking. Post-incubation, the supernatant was saved and the beads were washed twice with 120 μl 50 mM Tris/HCl, pH 7.5 containing 1 M urea. The supernatants were combined with the trypsin digest. To the pooled sample, DTT was added to a final concentration of 4 mM, and the sample was incubated at 25°C for 30 min with shaking. Iodoacetamide was added to a final concentration of 10 mM and the sample was incubated at 25°C for 45 min with shaking in the dark. Subsequently, an additional 1 μg of trypsin was added, and the second digestion was allowed to proceed overnight at 25°C with continuous shaking. The combined digested peptides were purified using home-made C18 stage tips.[63]

LC-MS/MS analysis

Liquid chromatography tandem mass spectrometry (LC-MS/MS) was performed on a nano-LC system (Ultimate 3000) coupled to an Impact II Q-TOF (Bruker Daltonics, Bremen, Germany) using a CaptiveSpray nano electrospray ionization (ESI) source as described previously.[64] Peptides (1 μg) were separated over a 30 min linear gradient of 5–45% (v/v) acetonitrile on a Acclaim Pepmap RSLC analytical column (C18, 100 Å, 75 μm x 50 cm) (Thermo Scientific). MS1 spectra with a mass range of m/z 200–2000 were acquired

at 3 Hz and the 18 most intense peaks were selected for MS/MS analysis with an intensity-dependent spectrum acquisition rate between 4 and 16 Hz. Dynamic exclusion duration was set to 0.5 minutes.

Raw data files were analyzed using MaxQuant software version 2.4.4.0,[54] with peak lists compared against the *Saccharomyces cerevisiae* reference proteome from UniProt (www.uniprot.org). All settings were kept at default values and protein quantification was performed using the label-free quantification (LFQ) algorithm.[65] Further analysis was performed using Perseus version 2.0.9.0.[55] Potential contaminants, proteins identified only through site modification, and reverse hits were removed. Only proteins quantifiable by the LFQ algorithm in at least two out of three replicates were kept. LFQ intensities were transformed to $\log_2$ values and missing data were imputed from a normal distribution within Perseus using standard parameters. Samples were statistically compared using a t-test and data was visualized using a custom RStudio[66] script.

Fluorescence microscopy

Yeast cells were grown in selective lactate medium containing 0.1% glucose ON at 30°C. On the next day, the cells were diluted into fresh selective lactate medium without any added sugar and grown till OD ca. 0.5. One sample per culture was directly imaged (0h) and the rest of the cultures were diluted to OD_{600} of 0.3 and expression of NS-mtGFP was induced by addition of galactose to 0.5%. If needed, the cultures were diluted in selective lactate medium containing 0.5% galactose so that OD_{600} remained between 0.3 and 0.8. After indicated time periods, 0.15 OD_{600} were isolated by centrifugation (3000 rcf, 3 min, RT), resuspended in 1 mL staining buffer (10 mM Hepes, pH 7.6, 5% glucose, sterile filtered) containing 50 nM Image-iT TMRM-Reagent (Thermo fisher) and rotated for 15 min at 30°C in the dark. Cells were re-isolated by centrifugation and washed two times with 1 mL staining buffer and once with 1 mL selective lactate medium containing 0.5% galactose. Cells were finally resuspended in 500 µl medium and 300 µl of the cell suspension were transferred into Concanavalin A coated 8-well chambered µ-slides with glass bottom (Ibidi). The cells were attached to Con A by a 2 min centrifugation of the slides at 800 rcf. Non-bound cells were subsequently washed three times with 400 µl medium. Images were captured in Z-stacks (41 slices, 200 nm) with a Nikon ECLIPSE Ti2-E microscope (Nikon MEA54000), with a CFI Apochromat TIRF 100XC oil immersion objective (Nikon MRD01991) and a Photometrics Prime 95B 25-mm camera (PH-P95B-25) at 30°C. The ND2 files of the NIS-ELEMENTS AR software (Nikon MQS31000) were converted to OME-TIFF using a custom Python 3 macro and deconvolved using Huygens Essential v 18.10 (Scientific Volume Imaging). Pictures in figures are presented as maximum intensity Z-projections created with Fiji/ImageJ. To allow for better visualization in case of the GFP channel pictures were equally and in case of the TMRM signal individually adjusted by setting the upper and lower borders of depicted pixel intensities. Single cells expressing GFP were manually cropped out using the Fiji ROI function and quantified with a custom Fiji/ImageJ macro. Briefly, the GFP channel of each cropped image was automatically analyzed for particles with the Fiji plugin "3D Objects Counter" ("slice=20 min.=7 max.=2562500 exclude_objects_on_edges objects surfaces statistics summary").[67] Initially, images were manually analyzed and evaluated to identify errors in the macro's performance. Subsequently, these erroneous analyses were automatically excluded by the macro using a predefined threshold. The data were then analyzed and plotted using custom Python scripts in Jupyter Notebook. Average values of three independent experiments with at least 150 cells per replicate were statistically compared using Student's t-test, as recommended by Lord et al. (2020)[68]

Pth2 antibody generation

Antibodies against Pth2 was generated in rabbits by injection of recombinantly expressed and purified His_6-Pth2(35-208). To validate the specificity of the obtained sera, total cell extracts from BY4742 and BY4742 *Δpth2* yeast cells were separated by SDS-PAGE, transferred to nitrocellulose membranes, and the obtained stripes used for western blot using preimmune and the sera obtained after immunization of the rabbits. Pth2-specific antibodies were affinity-purified from the sera using an affinity column made by coupling the same His_6-Pth2(35–208) fragment to CNBr-activated Sepharose 4B beads (Cytiva).

QUANTIFICATION AND STATISTICAL ANALYSIS

Details of the quantification and statistical analyses are provided in the respective STAR Methods sections, Figures and Figure legends. p-values are stated in the respective Figures. The antibody decorations as well as the serial dilution spot assays shown are representative results of at least three biological replicates.